

Chapter 4

Collection Optics Design for QFI

Two-Part Architecture, ETW Characterization, and Photonic Integration

This chapter develops the **optical collection component** of the measurement operator \mathcal{M} . The fundamental task is **two-part signal routing**: separating spatial registration (pointer optics) from photon harvesting (collection optics) to enable independent optimization of each function.

Key Achievements:

- Two-part architecture decoupling ETW-optimized pointing from NA-optimized collection
- Telecentric pointer optics for depth-invariant spatial registration with $ETW < 300 \text{ nm}$
- High-NA collection ($NA \geq 0.8$) for maximum photon throughput
- Uniform PSF across FOV ($\sigma_{\text{PSF}}/\overline{\text{PSF}} < 23\%$) for $\Gamma_{\text{mm}} > 0.95$

QFI Pipeline Position: $S \xrightarrow{\mathcal{G}} F \xrightarrow{\boxed{\mathcal{M}}} D \xrightarrow{\mathcal{R}} \hat{S}$

Abbreviated Terms

Abbrev.	Definition	Abbrev.	Definition
CRA	Chief Ray Angle	DOF	Depth of Field
ESF	Edge Spread Function	ETW	Edge Transition Width
FOV	Field of View	LSC	Laser Scanning Confocal
LSF	Line Spread Function	MTF	Modulation Transfer Function
NA	Numerical Aperture	NV	Nitrogen-Vacancy center
OPD	Optical Path Difference	OTF	Optical Transfer Function
PIC	Photonic Integrated Circuit	PSF	Point Spread Function
Q-OTF	Quantum OTF	QFI	Quantum Field Imaging
QFM	Quantum Field Metrology	RMS	Root Mean Square
SDC	Spinning Disk Confocal	SIM	Structured Illumination
SIL	Solid Immersion Lens	SNR	Signal-to-Noise Ratio
SQL	Standard Quantum Limit	WFE	Wavefront Error

Abstract

This chapter develops the optical collection system for Quantum Field Imaging, corresponding to the **measurement operator** \mathcal{M} in the QFI operator stack. We introduce a **two-part architecture** separating pointer optics (spatial registration) from collection optics (photon harvesting), enabling independent optimization. The **Edge Transition Width (ETW)** is established as the primary figure of merit for semiconductor applications, replacing traditional MTF metrics. We prove the **Snout Impossibility Theorem** demonstrating that conventional objectives cannot meet QFI requirements, necessitating compound designs. Comprehensive

treatment of **telecentric design**, **confocal feasibility**, and **photonic integration** pathways provides a complete framework from laboratory to production. The chapter concludes with entangled state collection theory for Heisenberg-limited sensitivity.

Clarification: Operator Taxonomy: Why Collection Optics Belongs to \mathcal{M}

Although optical propagation is sometimes treated as part of the forward model in classical imaging, in QFI we classify collection optics as part of the **measurement operator** \mathcal{M} , not the forward physics operator \mathcal{G} :

- \mathcal{G} (Forward Model): Maps sources $S(\mathbf{r})$ to physical fields $F(\mathbf{r})$ through physics (Biot-Savart, thermal diffusion, elasticity)
- \mathcal{M} (Measurement): Maps physical fields $F(\mathbf{r})$ to discrete data D through optics, quantum control, and statistical estimation

Collection optics directly shapes the PSF, determines the ETW, controls photon statistics, and therefore defines Γ_{mm} —all characteristics of how we *measure* the field, not how the field is *generated* by sources.

Part A: Foundations and Architecture

4.1 Introduction: Why Collection Optics Determines QFI Success

4.1.1 Historical Background

The development of high-performance collection optics has been central to microscopy since Abbe's resolution theory (1873). Key milestones include:

- **1873:** Abbe establishes resolution limit $d = \lambda/(2NA)$
- **1930s:** Oil-immersion objectives achieve $NA > 1.0$
- **1957:** Minsky patents confocal microscope
- **1980s:** Confocal microscopy enables depth sectioning
- **2000:** Gustafsson introduces structured illumination microscopy
- **2010s:** Solid immersion lenses for NV collection
- **2020s:** Quantum-enhanced microscopy and photonic integration

For QFI, collection optics must satisfy constraints unknown in classical microscopy: the “snout” geometry (working inside a magnet bore), multi-site phase-coherent collection, and compatibility with cryogenic environments.

4.1.2 Pain Points in Current Approaches

Practically we need to know what are the pain points in current approaches. We also need to understand the possible root causes and their impacts to the key features in quantum aspect. A brief table is used to highlight the key pain points as given below.

Table 4.1: Collection optics pain points for QFI systems.

Pain Point	Root Cause	Impact on Q_{FOM}
Low collection efficiency	Limited NA due to geometry	Direct throughput loss
PSF non-uniformity	Field-dependent aberrations	Γ_{mm} degradation
Poor edge localization	Wrong FOM (MTF vs. ETW)	Misaligned detection
Alignment drift	Bulk optics instability	Production reliability
No depth selectivity	Widefield imaging	Layer ambiguity in ICs
Serial scanning	Point-by-point confocal	Throughput bottleneck

4.1.3 Chapter Figures of Merit

Technically key features are characterized by figure of merit (FOM). The first 5 FOM is given below as reference.

Table 4.2: Primary figures of merit for collection optics design.

FOM	Symbol	Target	Impact
Edge Transition Width	ETW	< 300 nm	Defect localization
Collection efficiency	η_{total}	> 5%	Q_{FOM} throughput
PSF uniformity	$\sigma_{\text{PSF}}/\bar{\text{PSF}}$	< 10%	$\Gamma_{\text{mm}} > 0.95$
Chief Ray Angle	CRA	< 0.5°	Multi-layer alignment
Working distance	WD	> 10 mm	Sample access

4.2 Two-Part Architecture: Pointer vs. Collection

4.2.1 Architectural Concept

To effectively solve the pain points, it would be more efficient to work with two-part architecture, i.e., we need pointer optics, not just simply light collection.

The fundamental insight enabling QFI collection design is that **spatial registration** (pointer optics) and **photon harvesting** (collection optics) have conflicting optimization targets:

Table 4.3: Conflicting requirements for pointer and collection optics.

Parameter	Pointer Optics	Collection Optics
Primary goal	Spatial registration	Photon throughput
Key FOM	ETW (edge sharpness)	Collection efficiency η
NA requirement	Moderate (0.3–0.5)	High (≥ 0.8)
Wavelength	Visible (alignment)	NIR (NV fluorescence)
Telecentricity	Mandatory	Not critical
DOF	Shallow (layer select)	Deep (throughput)

In short, we have

Definition 4.2.1 (Two-Part Architecture). A collection system design that separates:

1. **Pointer optics:** Low-to-moderate NA, telecentric, ETW-optimized for spatial registration
2. **Collection optics:** High NA, efficiency-optimized for NV fluorescence harvesting

The two paths can be combined via dichroic beam splitters or spatial separation. Photonic integration can be a more effective solution for mass production.

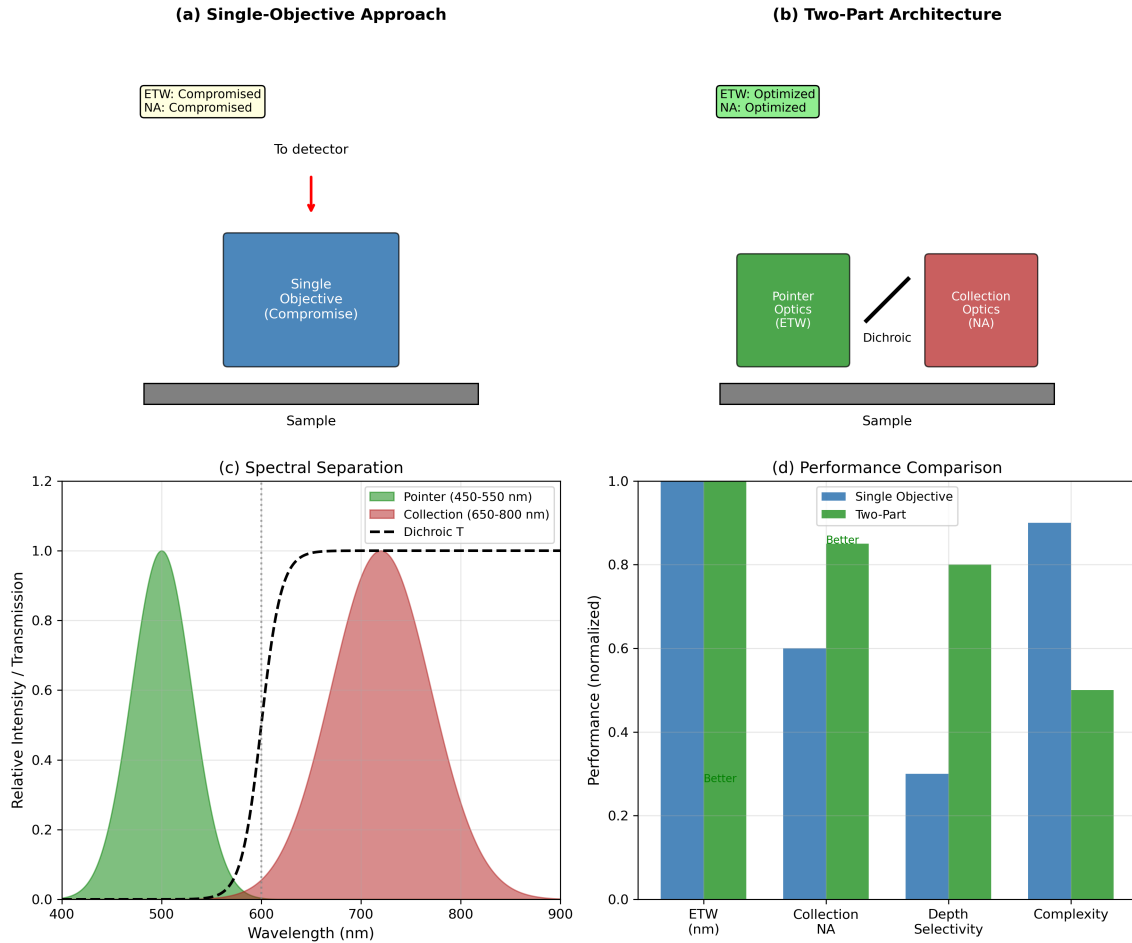


Figure 4.1: Two-part architecture concept. (a) Single-objective approach showing compromise between competing requirements. (b) Two-part architecture with independent optimization paths. (c) Spectral separation using dichroic beam splitter. (d) Performance comparison showing improvement in both ETW and collection efficiency.

4.2.2 Pointer Optics Requirements

The pointer optics subsystem prioritizes spatial registration accuracy:

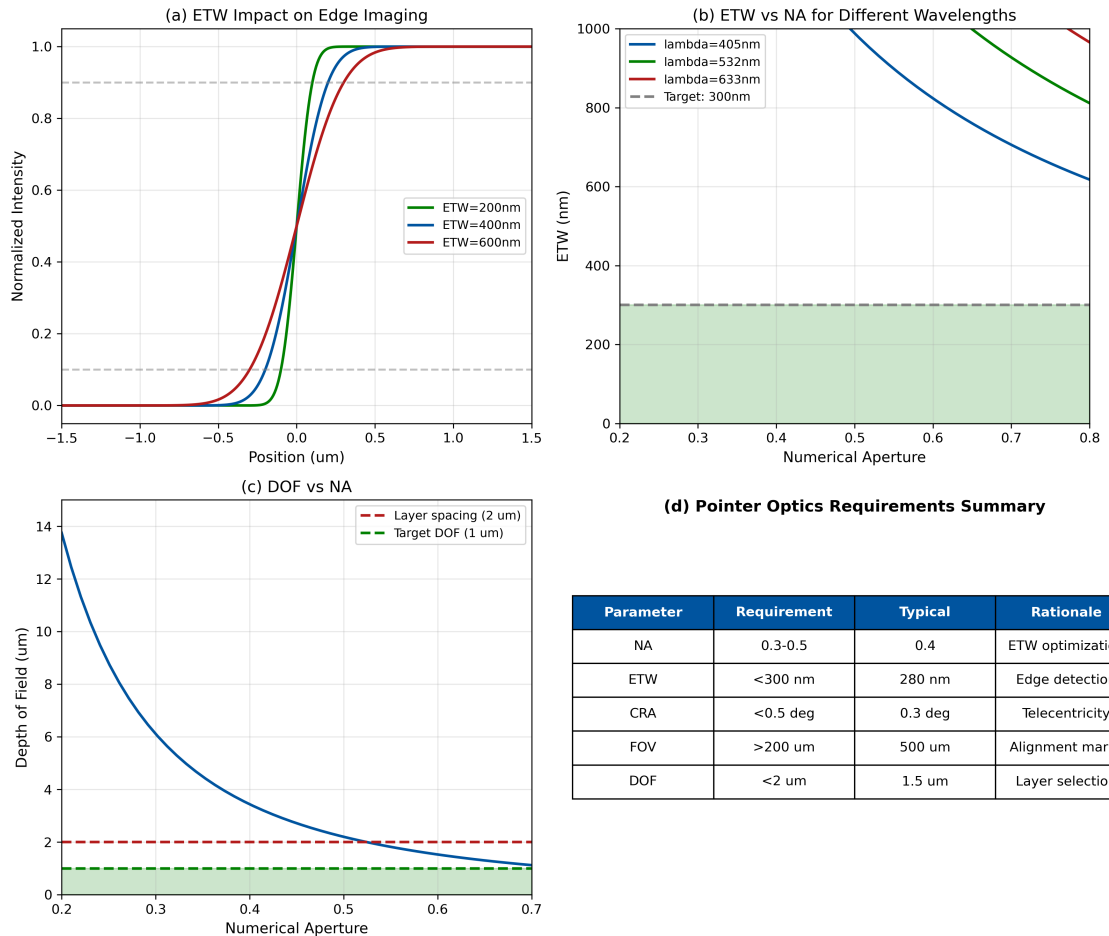


Figure 4.2: Pointer optics requirements. (a) ETW impact on edge imaging for different values (200, 400, 600 nm). (b) ETW vs. NA trade-off for different wavelengths (405, 532, 633 nm) with 300 nm target. (c) Depth of field vs. NA showing layer spacing constraint. (d) Requirements summary table.

Table 4.4: Pointer optics requirements for QFI.

Parameter	Requirement	Rationale	Typical
NA	0.3–0.5	ETW optimization	0.4
Telecentricity	< 0.5° CRA	Depth-invariant mag.	0.3°
ETW	< 300 nm	Sub-μm edge detection	280 nm
FOV	> 200 μm	Alignment mark coverage	500 μm
DOF	< 2 μm	Layer selection	1.5 μm

Design Rule 4.2.1: Pointer DOF for Layer Selection

For unambiguous layer identification in multi-metal ICs:

$$\text{DOF} < 0.5 \times \Delta z_{\text{layer}} \quad (4.1)$$

where Δz_{layer} is the minimum inter-layer spacing (typically 2–4 μm).

4.2.3 Architecture Comparison

Effectively two-part architecture is characterized in spectral or spatial domains which will give different performance and complexity.

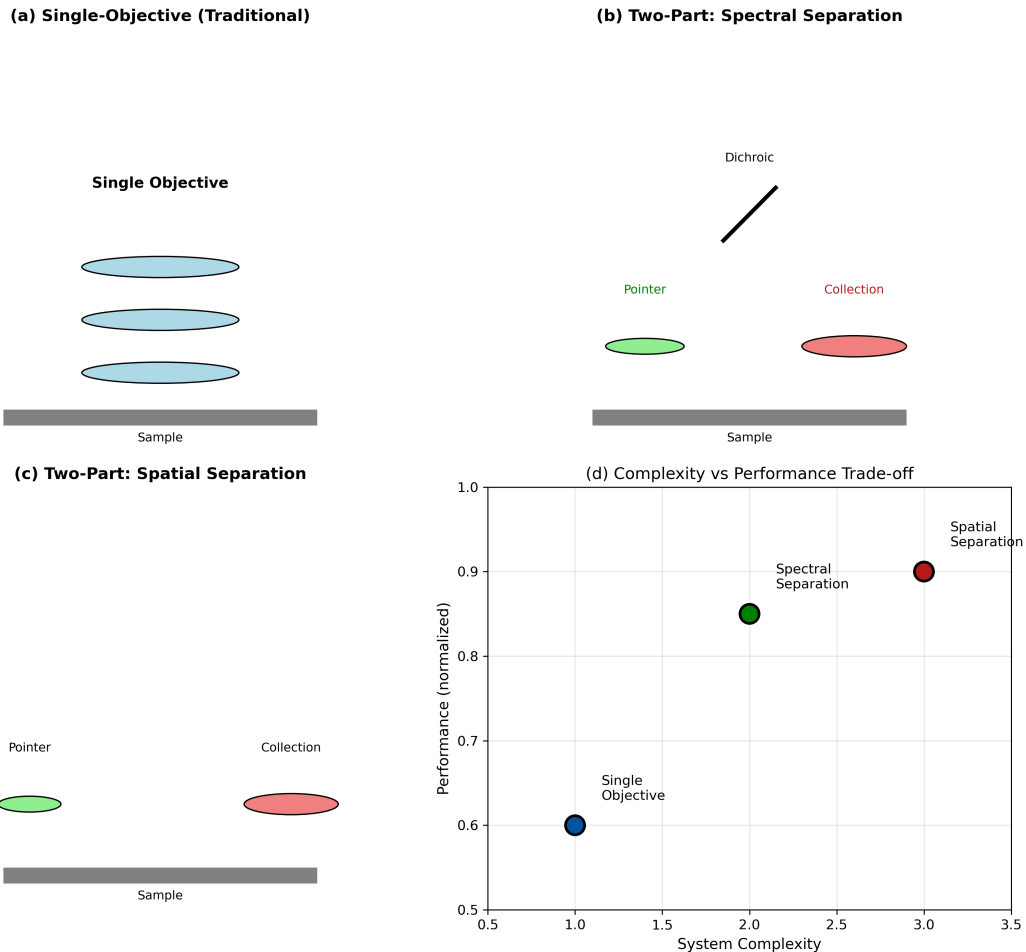


Figure 4.3: Architecture comparison. (a) Single-objective (traditional) layout. (b) Two-part with spectral separation via dichroic. (c) Two-part with spatial separation using separate objectives. (d) Trade-off analysis: complexity vs. performance for each architecture.

4.2.4 Two-Part Architecture: Failure Modes and Mitigations

Warning: Critical Failure Modes in Two-Part Architecture

The separation of pointer and collection paths introduces failure modes that must be addressed in production systems:

1. Cross-Path Chromatic Focus Mismatch

- *Cause:* Pointer (450–550 nm) and collection (650–800 nm) wavelengths have different focal planes due to glass dispersion
- *Mitigation:* Achromatic relay design; active focus compensation

2. Dichroic Angle Dependence

- *Cause:* Dichroic coating spectral response shifts with AOI (~ 0.1 nm per degree)
- *Mitigation:* Use dichroic in collimated space; specify $\text{AOI} < 5^\circ$

3. Independent Drift Decoupling

- *Cause:* Pointer and collection paths drift independently
- *Mitigation:* Common mounting structure; athermal materials (Invar, CFRP)

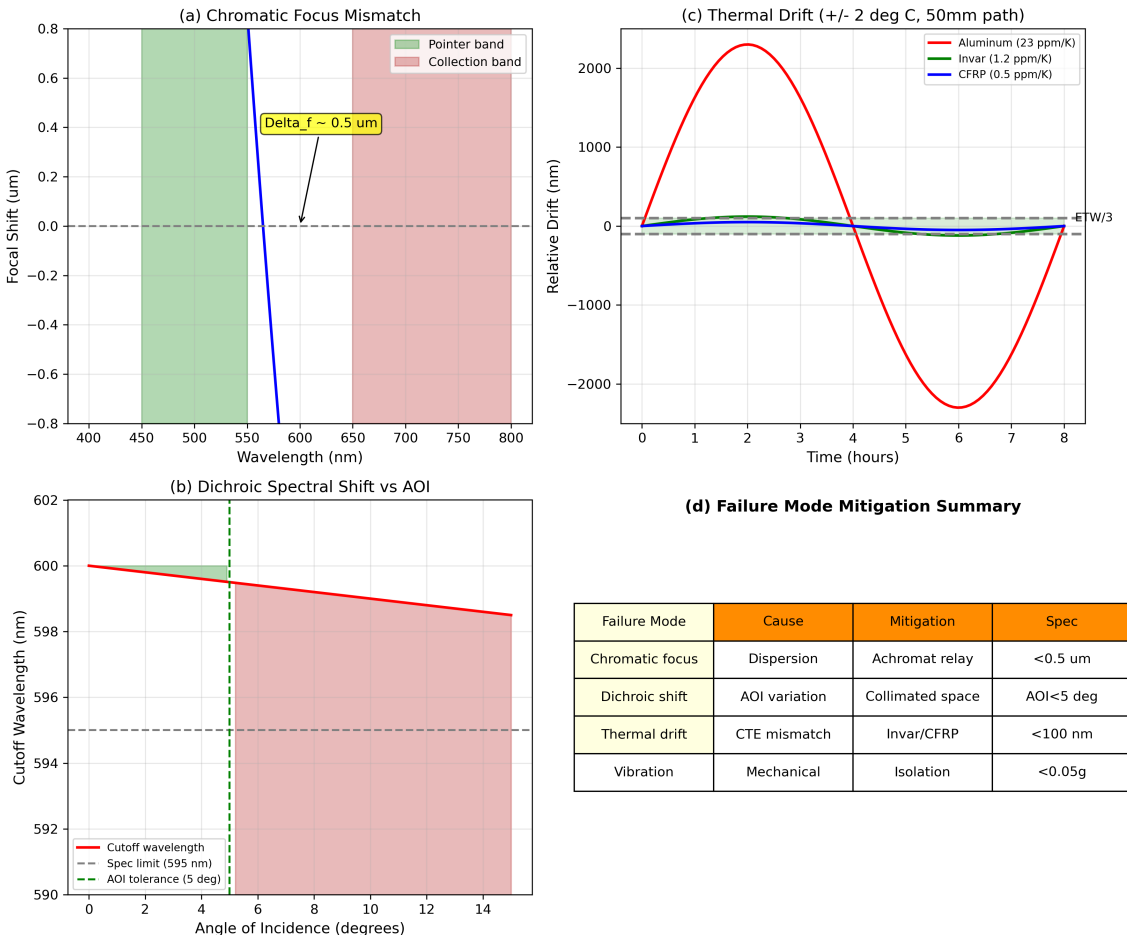


Figure 4.4: Two-part architecture failure modes. (a) Chromatic focus mismatch between pointer and collection bands showing $\Delta f \sim 0.5 \mu\text{m}$. (b) Dichroic spectral shift vs. angle of incidence with 5° tolerance specification. (c) Thermal drift comparison: aluminum ($\pm 2300 \text{ nm}$) vs. Invar ($\pm 120 \text{ nm}$) vs. CFRP ($\pm 50 \text{ nm}$) for $\pm 2^\circ\text{C}$ variation. (d) Failure mode mitigation summary table.

Design Rule 4.2.2: Two-Part Architecture Drift Budget

For production QFI systems with two-part architecture:

$$\Delta x_{\text{drift}} < \frac{\text{ETW}}{3} \approx 100 \text{ nm} \quad (4.2)$$

over 8-hour operating period. Requires temperature stability $\pm 1^\circ\text{C}$ and mounting CTE $< 2 \text{ ppm/K}$.

4.3 Edge Transition Width: The Primary FOM

4.3.1 Why MTF is Insufficient

The Modulation Transfer Function (MTF) characterizes response to sinusoidal patterns—appropriate for periodic structures but suboptimal for semiconductor FA where **edge-based structures** dominate: current paths with sharp boundaries, via arrays with discrete locations, and defects creating localized discontinuities.

Definition 4.3.1 (Edge Transition Width). The Edge Transition Width (ETW) is defined as the spatial distance over which the imaged intensity transitions from 10% to 90% of full contrast when imaging a perfect step edge:

$$\text{ETW} = x_{90\%} - x_{10\%} \quad (4.3)$$

ETW directly predicts edge localization uncertainty: $\sigma_{\text{edge}} \approx \text{ETW}/\sqrt{12}$ for photon-noise-limited detection with threshold-based edge localization.

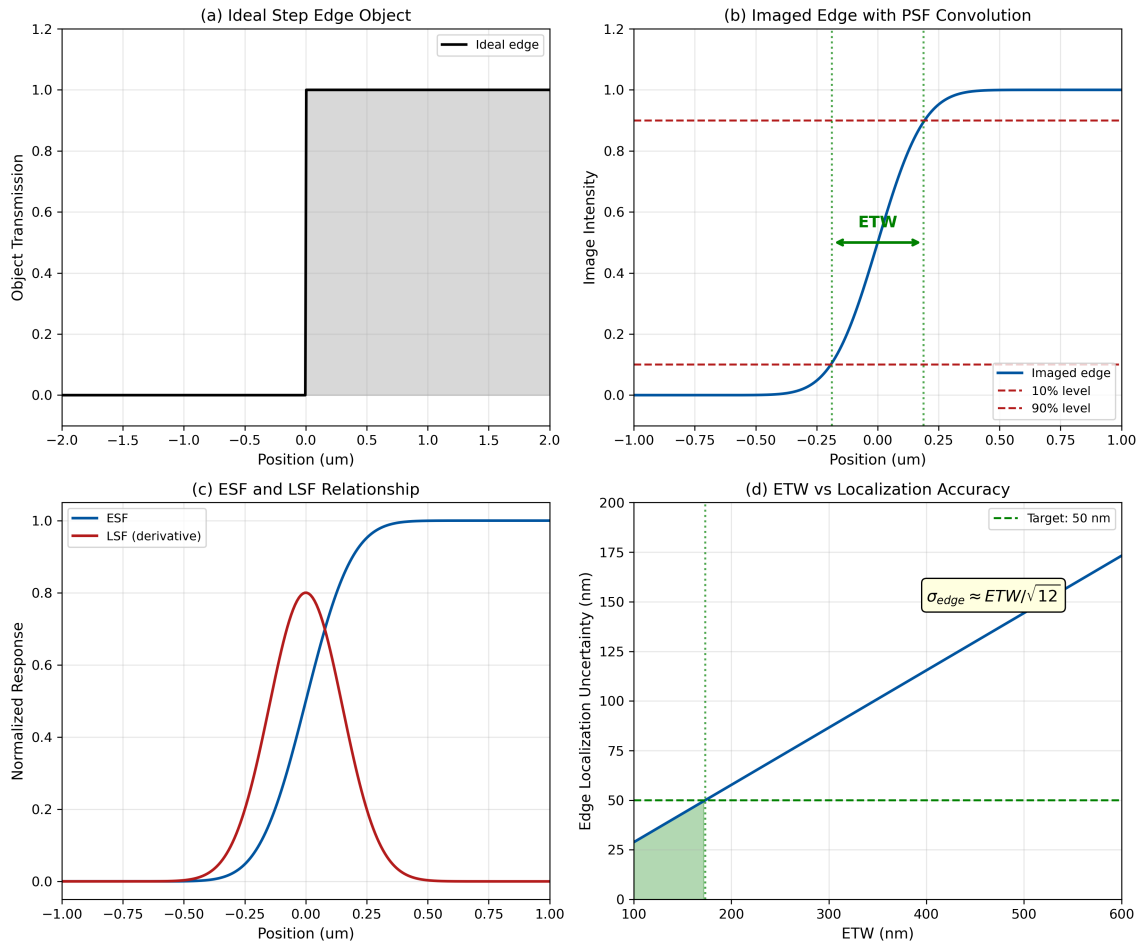


Figure 4.5: Edge Transition Width definition. (a) Ideal step edge object with unit transmission change. (b) Imaged edge showing PSF convolution effect with 10%–90% transition marked. (c) ESF and LSF relationship through differentiation. (d) ETW vs. edge localization uncertainty relationship.

4.3.2 ETW Fundamental Equation

Key Equation: ETW-PSF Relationship

For an aberration-free optical system with incoherent illumination:

$$\text{ETW} = 2 \int_0^{\infty} \text{PSF}(r) \cdot r \, dr \approx 1.22 \times \frac{\lambda}{\text{NA}} \quad (4.4)$$

This equals the Airy disk diameter for diffraction-limited optics.

Clarification: Assumptions for Equation 4.4

The ETW approximation $\text{ETW} \approx 1.22\lambda/\text{NA}$ assumes:

1. **Incoherent illumination:** Intensities add (not amplitudes)
2. **Uniform circular pupil:** No apodization or central obscuration
3. **Aberration-free imaging:** Diffraction-limited ($\text{Strehl} > 0.8$)
4. **Threshold-based detection:** 10–90% transition definition

Coherent illumination modifies the prefactor but preserves λ/NA scaling.

4.3.3 ETW and MTF: Mathematical Equivalence

Clarification: ETW vs. MTF: Fourier Domain Relationship

ETW and MTF are mathematically equivalent through the Fourier relationship:

- **Edge Spread Function (ESF):** Direct measurement of step edge response
- **Line Spread Function (LSF):** $\text{LSF}(x) = \frac{d}{dx} \text{ESF}(x)$
- **Optical Transfer Function (OTF):** $\text{OTF}(k) = \mathcal{F}\{\text{LSF}(x)\}$
- **Modulation Transfer Function (MTF):** $\text{MTF}(k) = |\text{OTF}(k)|$

Our choice of ETW is an **application-driven metric selection**: semiconductor FA involves edge-based structures where spatial-domain characterization provides more intuitive design guidance.

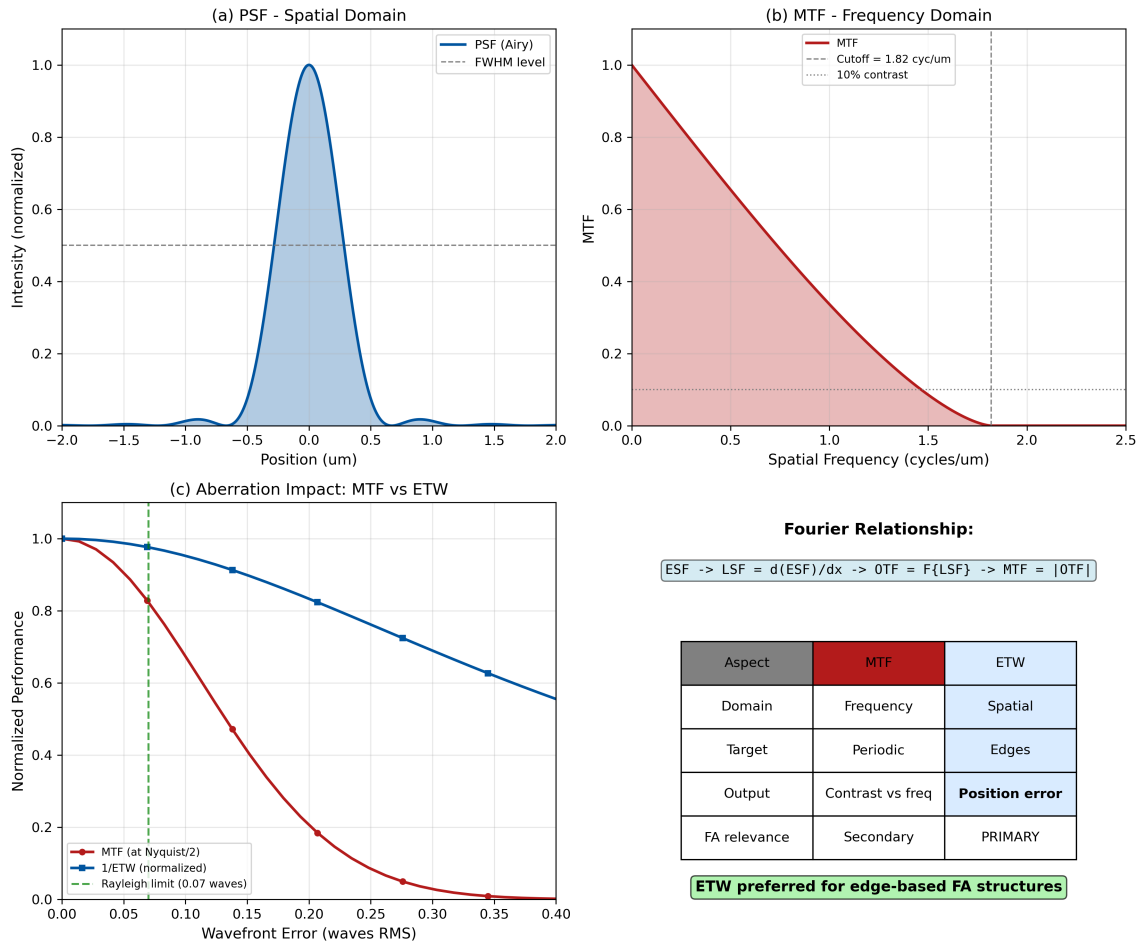


Figure 4.6: ETW vs. MTF comparison. (a) PSF (Airy pattern) in spatial domain. (b) MTF in frequency domain with cutoff at $2\text{NA}/\lambda$. (c) Aberration impact comparison: MTF degradation vs. ETW increase. (d) Comparison table and Fourier relationship showing mathematical equivalence.

Design Rule 4.3.1: ETW Requirement for Current Path Detection

For reliable edge detection of current paths with width w :

$$\text{ETW} < \frac{w}{3} \quad (4.5)$$

This ensures path edges are resolved with $> 80\%$ contrast. For modern IC paths ($w \approx 1 \mu\text{m}$), this requires $\text{ETW} < 300 \text{ nm}$.

4.4 Telecentric Design for Pointer Optics

4.4.1 Why Telecentricity is Mandatory

For QFI pointer optics, telecentricity is **mandatory** for accurate spatial registration across IC metal layers with different z-depths.

Definition 4.4.1 (Telecentric Optical System). An optical system is telecentric when the chief ray is parallel to the optical axis in either object space (object-side telecentric), image space (image-side telecentric), or both (bi-telecentric). For QFI, **object-side telecentricity** is essential.

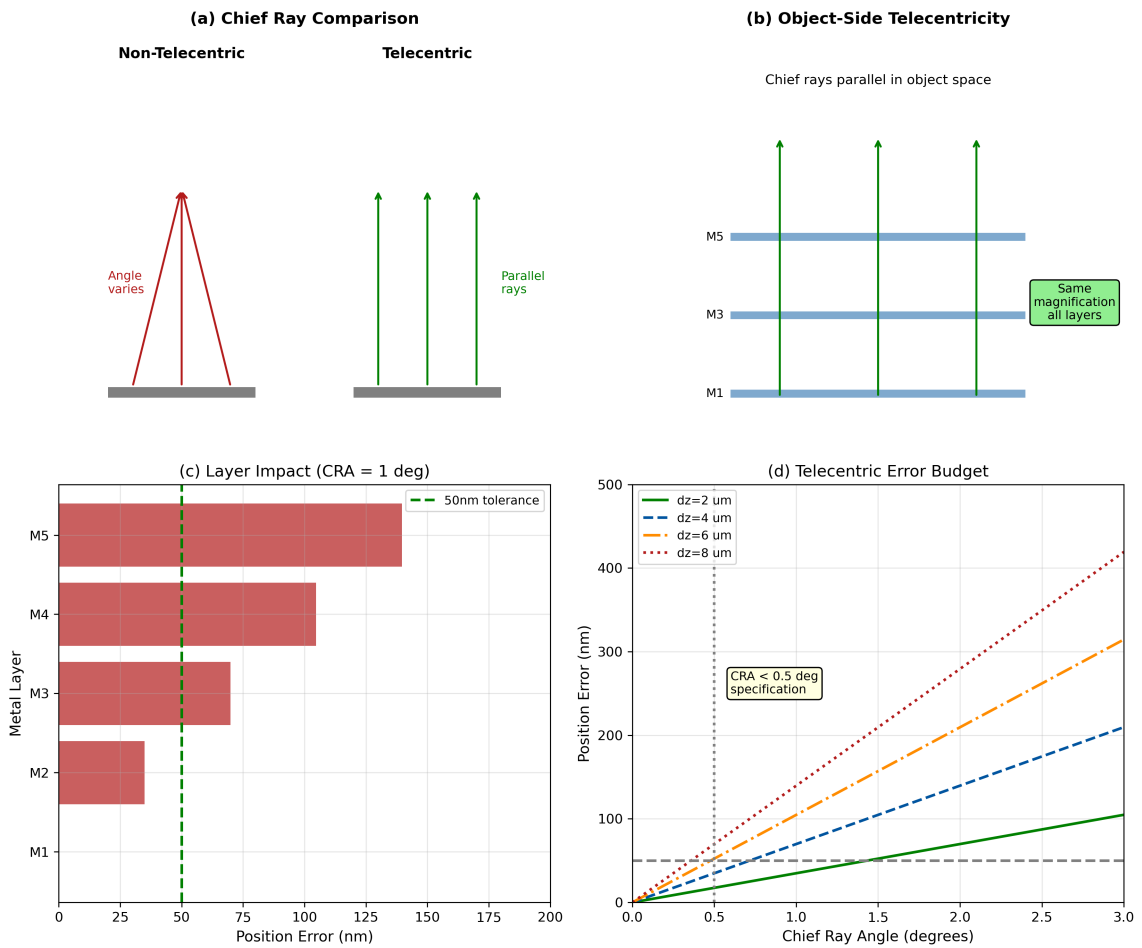


Figure 4.7: Telecentricity requirement. (a) Non-telecentric vs. telecentric chief ray comparison. (b) Object-side telecentricity with parallel chief rays enabling depth-invariant magnification. (c) Layer impact of non-telecentricity showing position error vs. metal layer. (d) CRA vs. position error budget for different depth ranges.

4.4.2 Telecentric Error Analysis

Key Equation: Telecentric Position Error

$$\Delta x_{\text{position}} = \Delta z \cdot \tan(\theta_{\text{CRA}}) \approx \Delta z \cdot \theta_{\text{CRA}} \quad (\text{paraxial, } \theta < 10^\circ) \quad (4.6)$$

Example 4.4.1 (Telecentric Error Budget). For IC alignment with $\Delta z = 2 \mu\text{m}$ layer spacing and target accuracy $\sigma_{\text{align}} < 50 \text{ nm}$:

$$\theta_{\text{CRA},\text{max}} = \frac{50 \text{ nm}}{2 \mu\text{m}} = 0.025 \text{ rad} = 1.43^\circ \quad (4.7)$$

With 3σ margin: $\theta_{\text{CRA}} < 0.5^\circ$ specification.

Design Rule 4.4.1: Telecentricity Specification

Pointer optics must achieve object-side telecentricity with:

$$\theta_{\text{CRA}} < 0.5^\circ \quad \text{across full FOV} \quad (4.8)$$

This ensures $< 50 \text{ nm}$ position error for $6 \mu\text{m}$ depth range in advanced ICs.

4.4.3 Double-Gauss Telecentric Design

The classical Double-Gauss configuration is the preferred starting point for QFI pointer optics due to its excellent balance of performance and complexity:

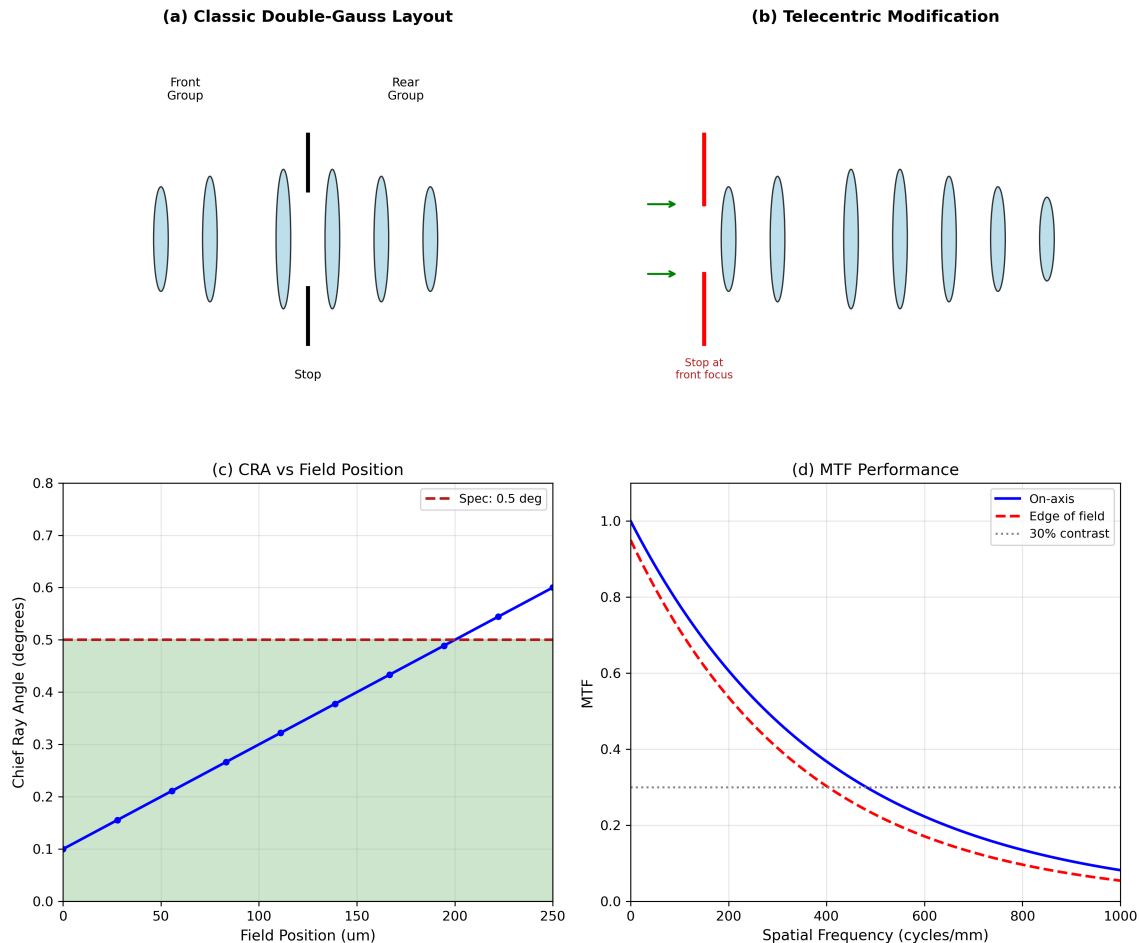


Figure 4.8: Double-Gauss telecentric design. (a) Classic Double-Gauss symmetric layout with central stop. (b) Modified configuration for object-side telecentricity with stop at front focal plane. (c) Ray trace showing CRA < 0.3° across field. (d) MTF and ETW performance curves.

4.4.4 Four-Group Telecentric Architecture

For demanding applications requiring longer working distance or higher NA, the four-group architecture provides additional design freedom:

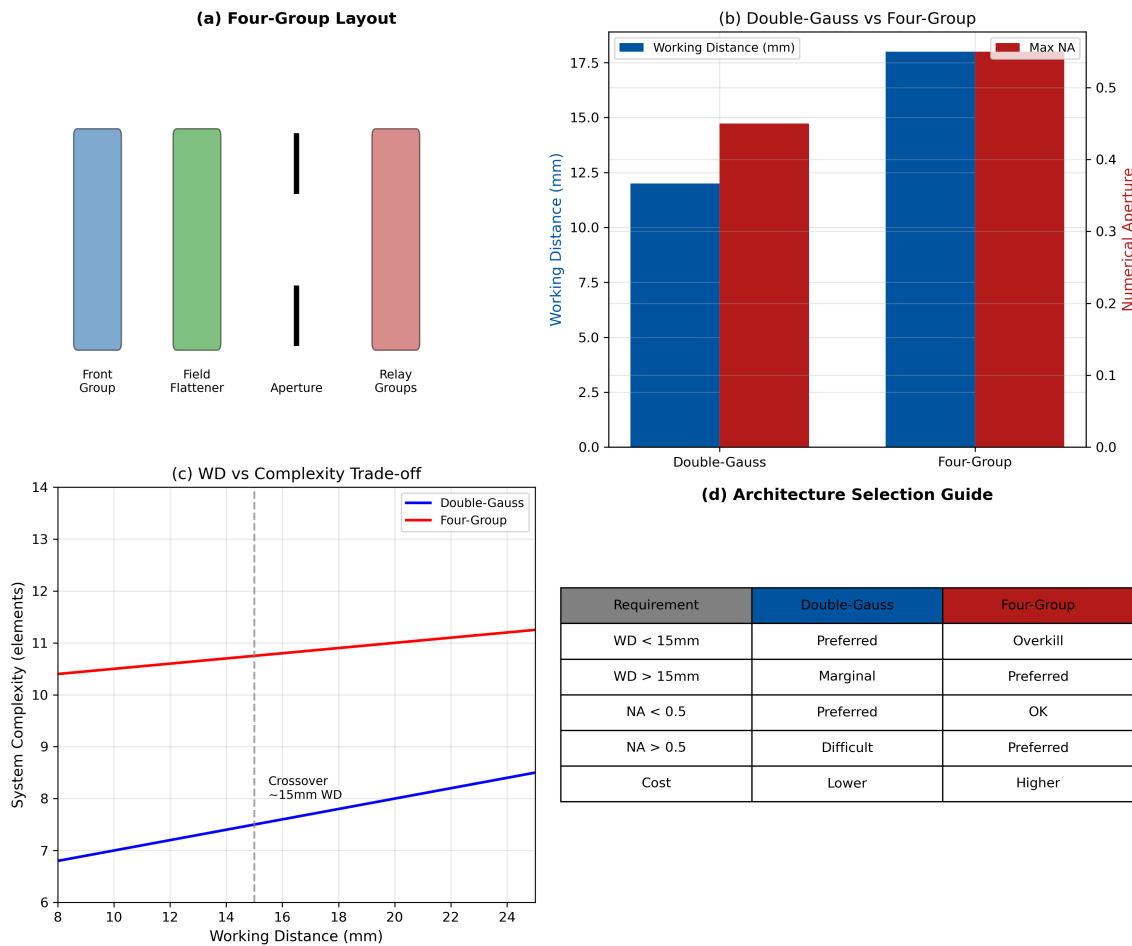


Figure 4.9: Four-group telecentric architecture. (a) General layout showing front group, field flattener, aperture, and relay groups. (b) Comparison with Double-Gauss for working distance and NA. (c) Working distance vs. complexity trade-off with crossover at ~ 15 mm. (d) Architecture selection guide table.

Design Rule 4.4.2: Telecentric Architecture Selection

Select telecentric architecture based on requirements:

- **Double-Gauss:** Default for $WD < 15$ mm, $NA < 0.5$
- **Four-group:** Use for $WD > 15$ mm or $NA > 0.5$

Both achieve $CRA < 0.5^\circ$ with proper optimization. Both already have vendors of high-quality lenses for system integration.

4.5 Confocal Feasibility for Depth Selectivity

4.5.1 The Depth Selectivity Problem

Widefield pointer optics image all IC layers simultaneously, creating ambiguity for multi-layer alignment. Confocal techniques provide optical sectioning.

Definition 4.5.1 (Optical Sectioning). The ability to selectively image a thin slice of the sample while rejecting out-of-focus contributions. Quantified by the **axial resolution** Δz_{FWHM} .

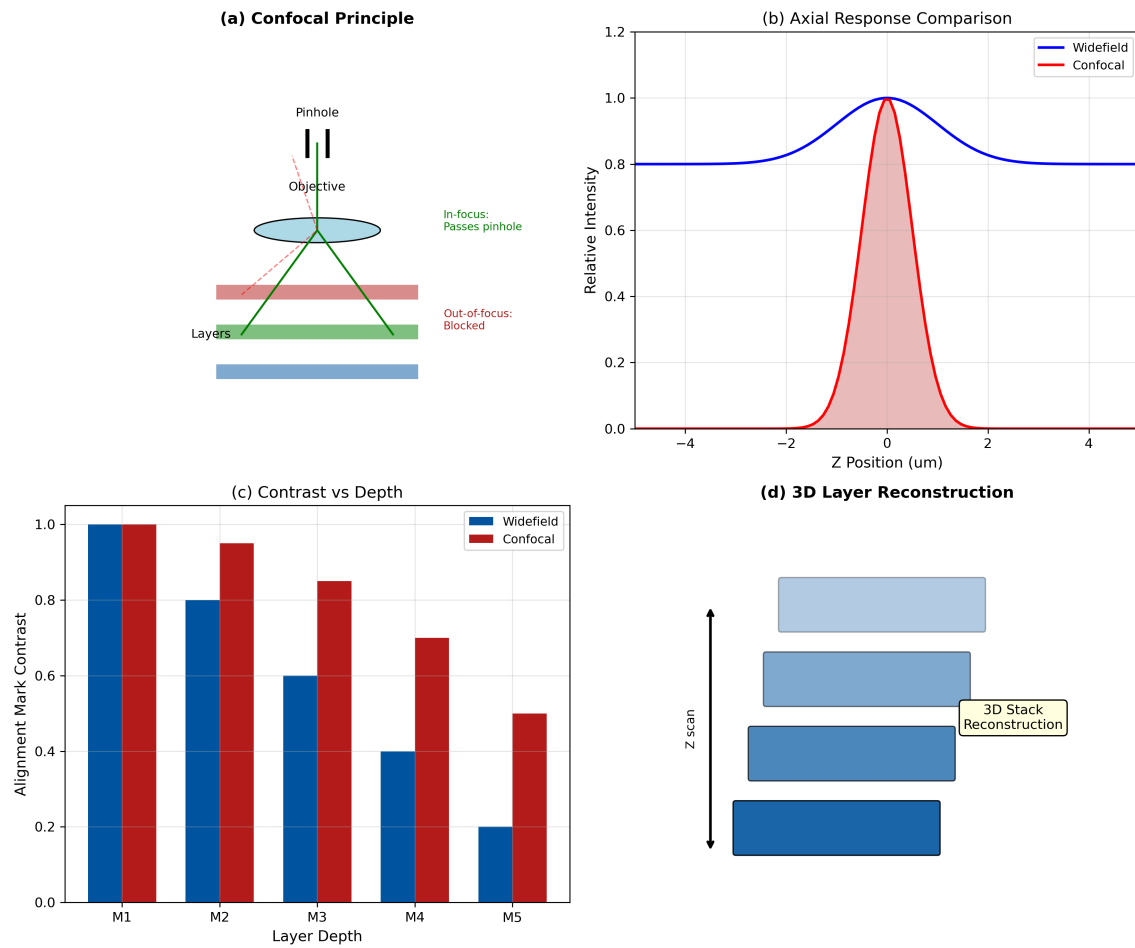


Figure 4.10: Confocal microscopy concept for QFI. (a) Confocal principle with pinhole rejecting out-of-focus light from different IC layers. (b) Axial response comparison: widefield (flat) vs. confocal (peaked). (c) Buried alignment mark contrast improvement with confocal. (d) 3D layer reconstruction concept from z-stack acquisition.

4.5.2 Confocal Configurations Comparison

Table 4.5: Confocal configuration comparison for QFI pointer optics.

Configuration	Speed	Sectioning	Complexity	QFI Fit
Laser Scanning (LSC)	Slow	Excellent	High	Calibration only
Spinning Disk (SDC)	Medium	Good	Medium	Production possible
Structured Illum. (SIM)	Fast	Good	Low	Recommended

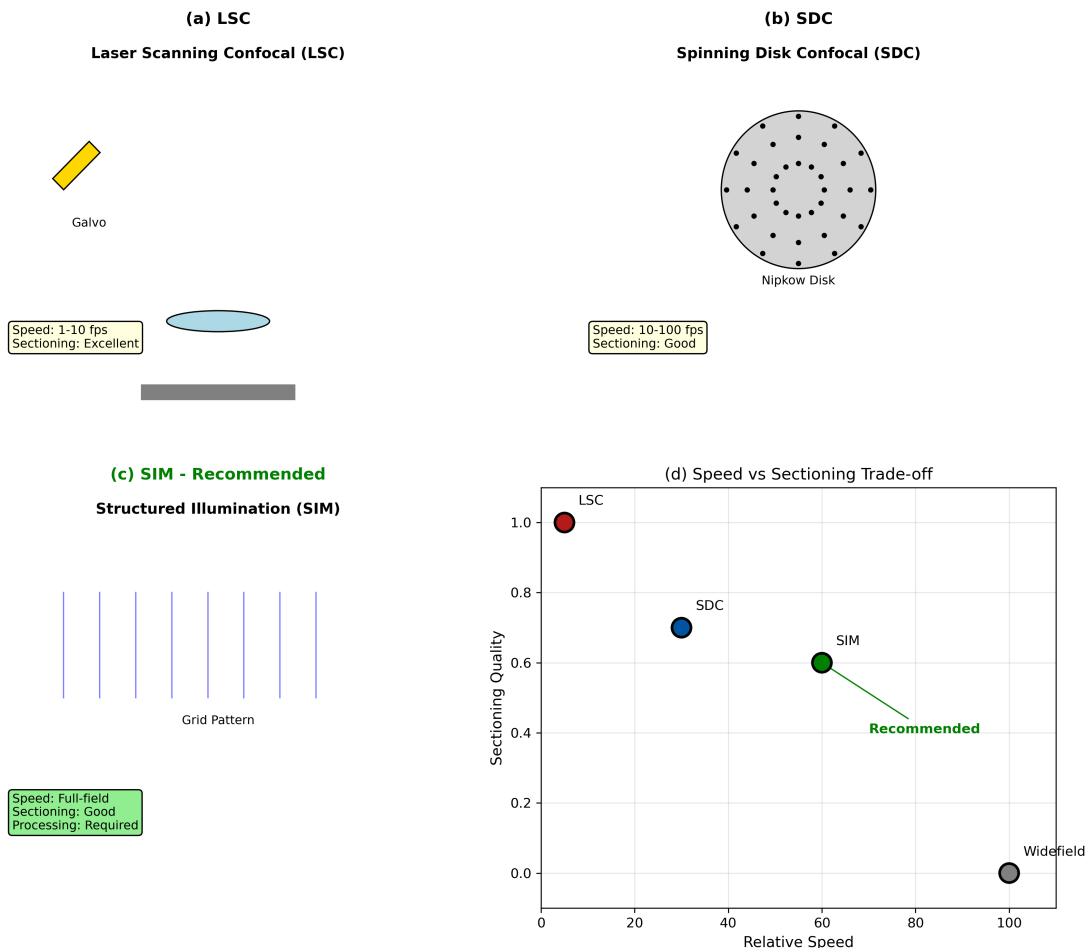


Figure 4.11: Confocal configuration comparison. (a) LSC schematic with galvo scanners—excellent sectioning but slow (1–10 fps). (b) SDC with Nipkow disk—good speed (10–100 fps) and sectioning. (c) SIM with grid pattern illumination—recommended for QFI. (d) Speed vs. sectioning quality trade-off with SIM highlighted.

4.5.3 SIM Photon Budget and Q_{FOM} Impact

Clarification: SIM Trade-off: Sectioning vs. Throughput

Structured Illumination requires multiple raw frames with shifted patterns, introducing a photon budget trade-off:

- **Raw frames:** 3–9 required vs. 1 for widefield
- **Axial resolution:** $\sim \lambda/\text{NA}^2$ ($2\times$ improvement)
- **Effective throughput:** $\sim 0.3\times$ widefield

Net Q_{IFOM} impact:

$$Q_{\text{IFOM},\text{SIM}} = Q_{\text{FOM},\text{widefield}} \times \frac{1}{3} \times \Gamma_{\text{inv}}(\text{improved}) \quad (4.9)$$

When layer ambiguity causes $\Gamma_{\text{inv}} < 0.3$, SIM improves overall Q_{IFOM} .

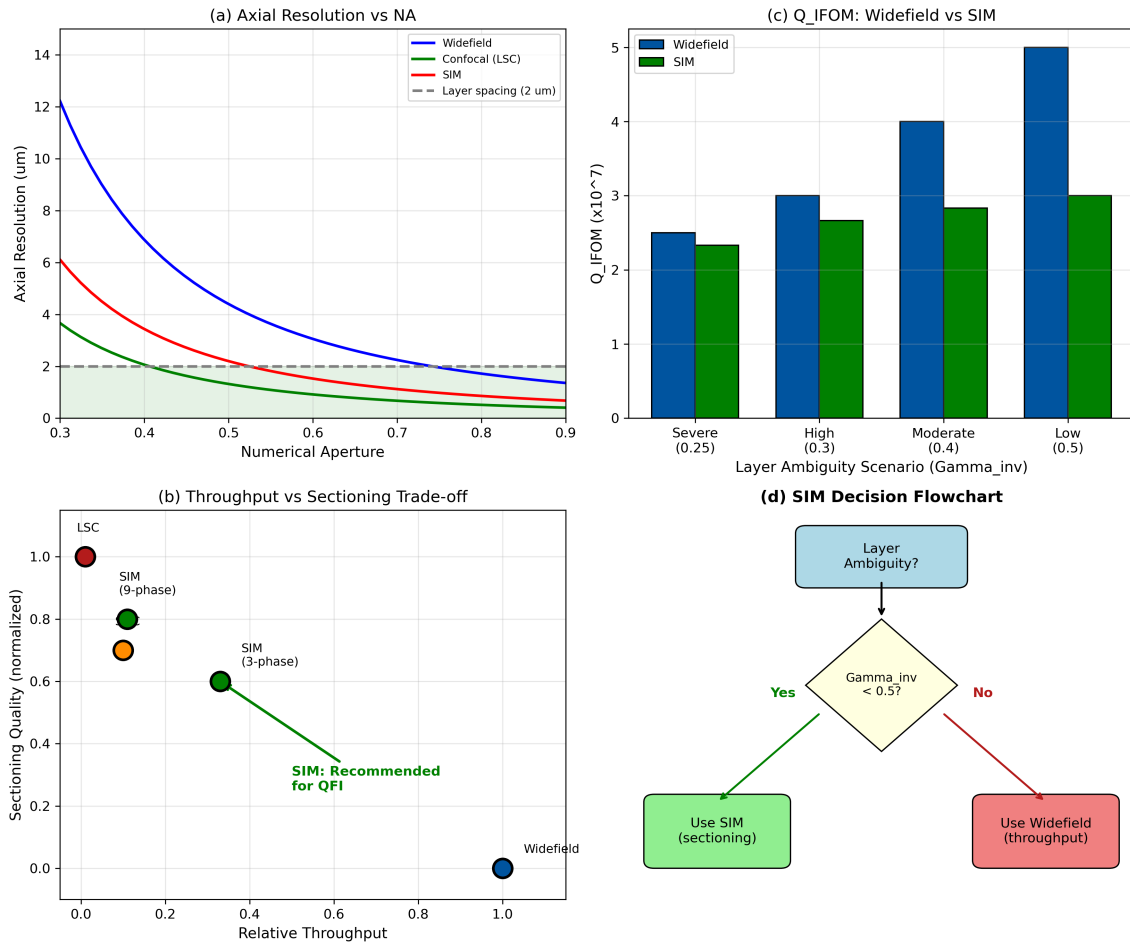


Figure 4.12: SIM throughput vs. sectioning trade-off. (a) Axial resolution vs. NA for widefield, confocal, and SIM with $2 \mu\text{m}$ layer spacing reference. (b) Throughput vs. sectioning scatter plot showing SIM as recommended compromise. (c) Q_{IFOM} comparison: SIM wins when layer ambiguity dominates ($\Gamma_{\text{inv}} < 0.5$). (d) Decision flowchart for SIM vs. widefield selection.

Design Rule 4.5.1: Confocal Recommendation for QFI

For multi-layer IC alignment requiring depth selectivity:

- **Recommended:** Structured Illumination (SIM)
- **Alternative:** Spinning Disk Confocal for superior sectioning
- **Specification:** Axial resolution $\Delta z < 0.5 \times$ layer spacing

Note: Confocal/SIM applies to **pointer optics only**, not collection optics.

Part B: Optical Design Fundamentals

4.6 Collection Efficiency Fundamentals

4.6.1 Solid Angle Collection

The collection efficiency for an isotropic emitter is determined by the solid angle subtended by the collection optics:

Key Equation: Collection Solid Angle

$$\eta_{\Omega} = \frac{\Omega}{4\pi} = \frac{1 - \cos(\theta_{\max})}{2} = \frac{1 - \sqrt{1 - \text{NA}^2/n^2}}{2} \quad (4.10)$$

where n is the refractive index and $\theta_{\max} = \arcsin(\text{NA}/n)$.

Table 4.6: Collection efficiency vs. numerical aperture (air, $n = 1$).

NA	θ_{\max}	η_{Ω}	Relative
0.4	23.6°	4.2%	0.33
0.6	36.9°	9.6%	0.75
0.8	53.1°	12.8%	1.00
0.9	64.2°	21.0%	1.64
1.0 (oil)	90.0°	50.0%	3.91

4.6.2 Diamond Interface Effects

NV centers emit from within diamond ($n = 2.4$), creating significant challenges:

- **Critical angle:** $\theta_c = \arcsin(1/2.4) = 24.6^\circ$
- **Total internal reflection:** 83% of emission trapped in diamond
- **Solid immersion lens (SIL):** Can recover trapped light

Key Equation: Total Collection Efficiency

$$\eta_{\text{total}} = \eta_{\Omega} \times T_{\text{Fresnel}} \times \eta_{\text{optics}} \times \eta_{\text{filter}} \times \eta_{\text{detector}} \quad (4.11)$$

Typical: $0.13 \times 0.85 \times 0.9 \times 0.8 \times 0.7 \approx 5.5\%$.

Remark 4.6.1 (NV Dipole Emission Anisotropy). The equations above assume isotropic emission. NV centers are electric dipole emitters with orientation-dependent emission patterns. For ensembles with random orientations, the isotropic approximation is valid to within 5%. Single-NV experiments require explicit dipole modeling.

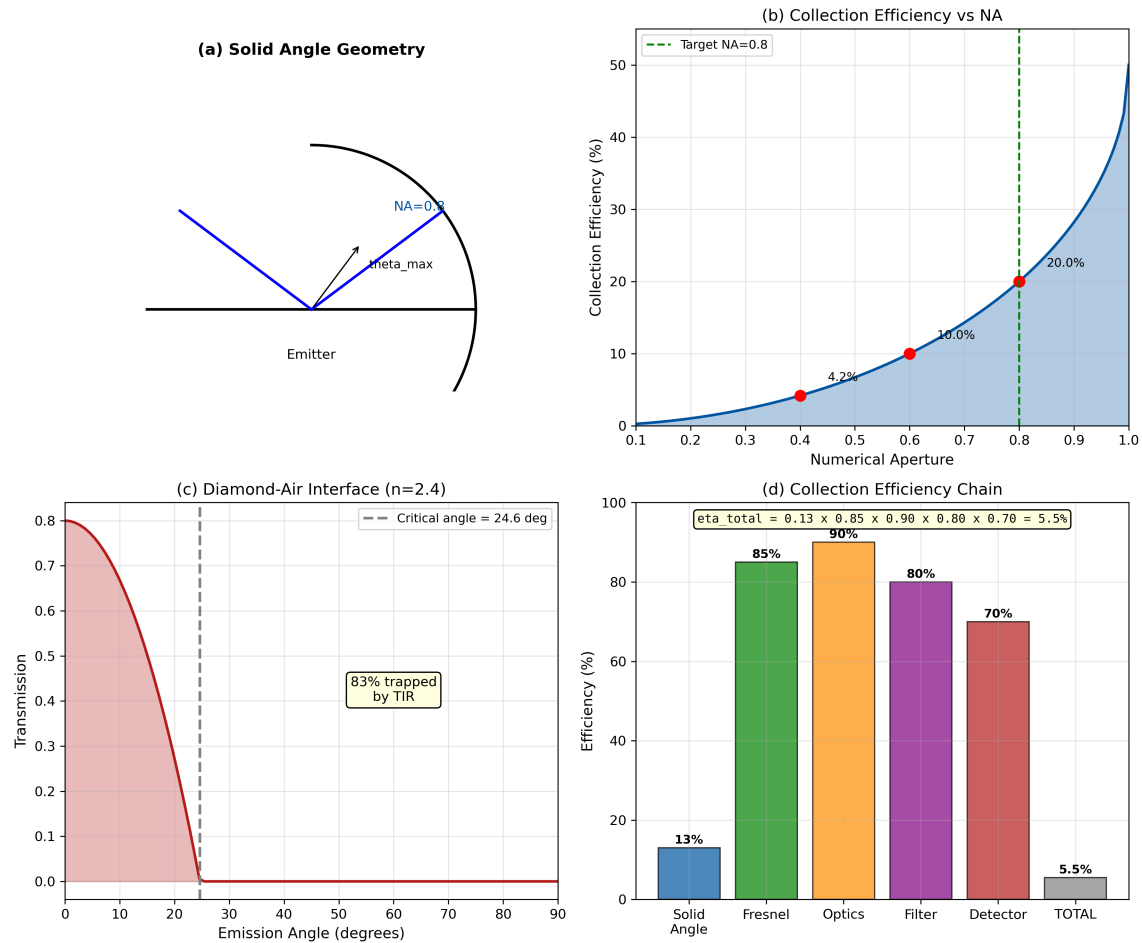


Figure 4.13: Collection efficiency fundamentals. (a) Solid angle geometry showing collection cone for NA=0.8. (b) Collection efficiency vs. NA curve with key points marked. (c) Diamond-air interface showing critical angle and TIR with 83% trapped light. (d) Total collection efficiency chain breakdown.

Design Rule 4.6.1: Collection Optics NA Threshold

For QFI throughput optimization:

$$NA_{collection} \geq 0.8 \quad (4.12)$$

This corresponds to > 12% solid angle collection. Lower NA results in direct Q_{FOM} degradation proportional to NA^2 .

4.7 The Snout Design Problem

4.7.1 Geometric Constraints

The “snout” is the collection optics assembly that must fit within the magnet bore of a QFI system:

Table 4.7: Snout geometric constraints for QFI systems.

Parameter	Constraint	Origin
Bore diameter	25–50 mm	Magnet design
Working distance	> 10 mm	Sample access
Envelope diameter	< 30 mm	Bore clearance
Total length	< 100 mm	System integration

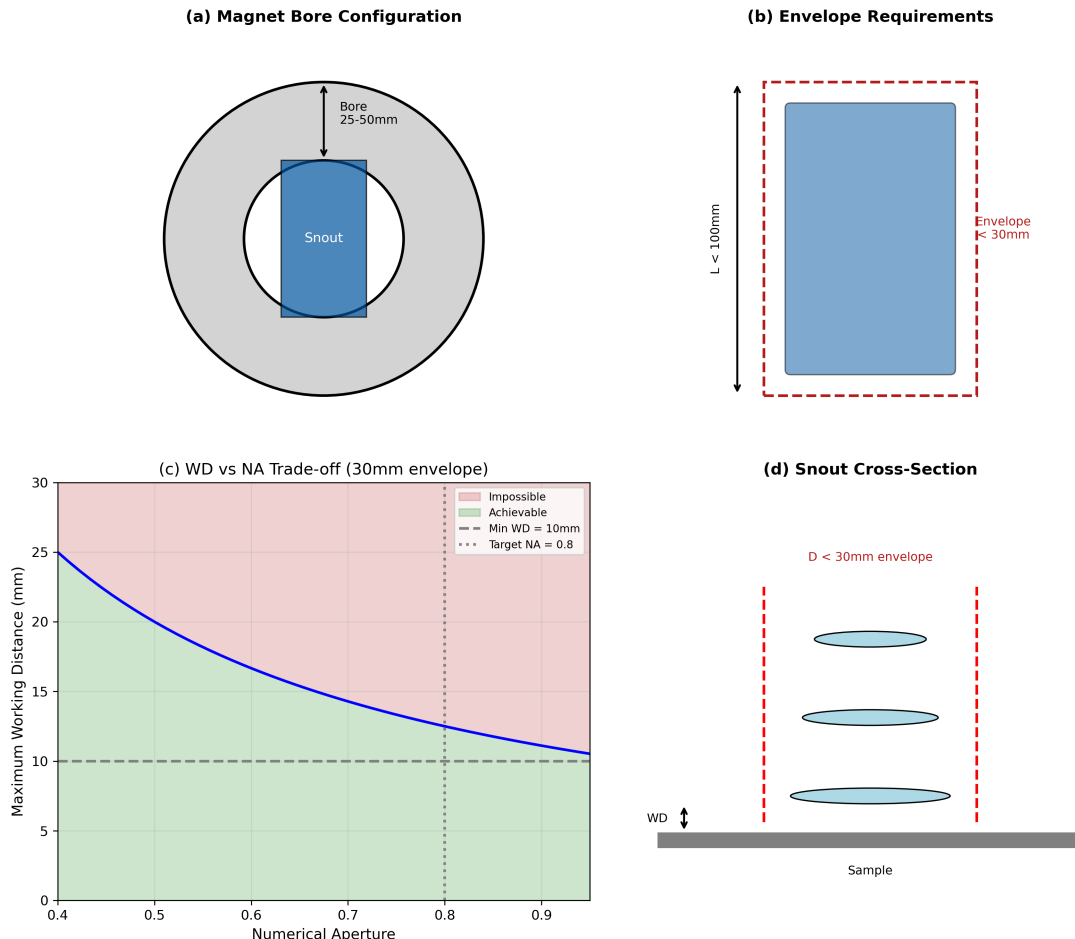


Figure 4.14: Snout geometry constraints. (a) Magnet bore cross-section with snout inside 25–50 mm bore. (b) Envelope requirements showing <30 mm diameter and <100 mm length limits. (c) Working distance vs. NA trade-off for 30 mm envelope. (d) Snout cross-section showing optical elements within geometric constraints.

4.7.2 The Snout Impossibility Theorem

It turns out we have geometric constraint when we use traditional on-shelf lens which has good vendor support.

Theorem 4.7.1 (Snout Impossibility—Geometric Constraint). *No single refractive objective can simultaneously achieve:*

1. $NA \geq 0.8$
2. *Working distance $WD \geq 10 \text{ mm}$*

3. Envelope diameter $D \leq 30 \text{ mm}$

with diffraction-limited performance over $\text{FOV} \geq 500 \mu\text{m}$.

This is a geometric ray constraint, not a limitation of aberration correction sophistication.

Proof. The edge ray height at the first optical surface is determined by the Lagrange invariant:

$$h_{\text{edge}} = \text{NA} \times \text{WD} \quad (4.13)$$

For $\text{NA} = 0.8$ and $\text{WD} = 10 \text{ mm}$: $h_{\text{edge}} = 8 \text{ mm}$.

This is a **geometric ray invariant** that cannot be circumvented by any lens design approach, including freeform surfaces, exotic materials, or diffractive elements. Including correction elements and mounting: minimum envelope $\geq 25 \text{ mm}$. With thermal margins, the 30 mm constraint cannot be satisfied. \square

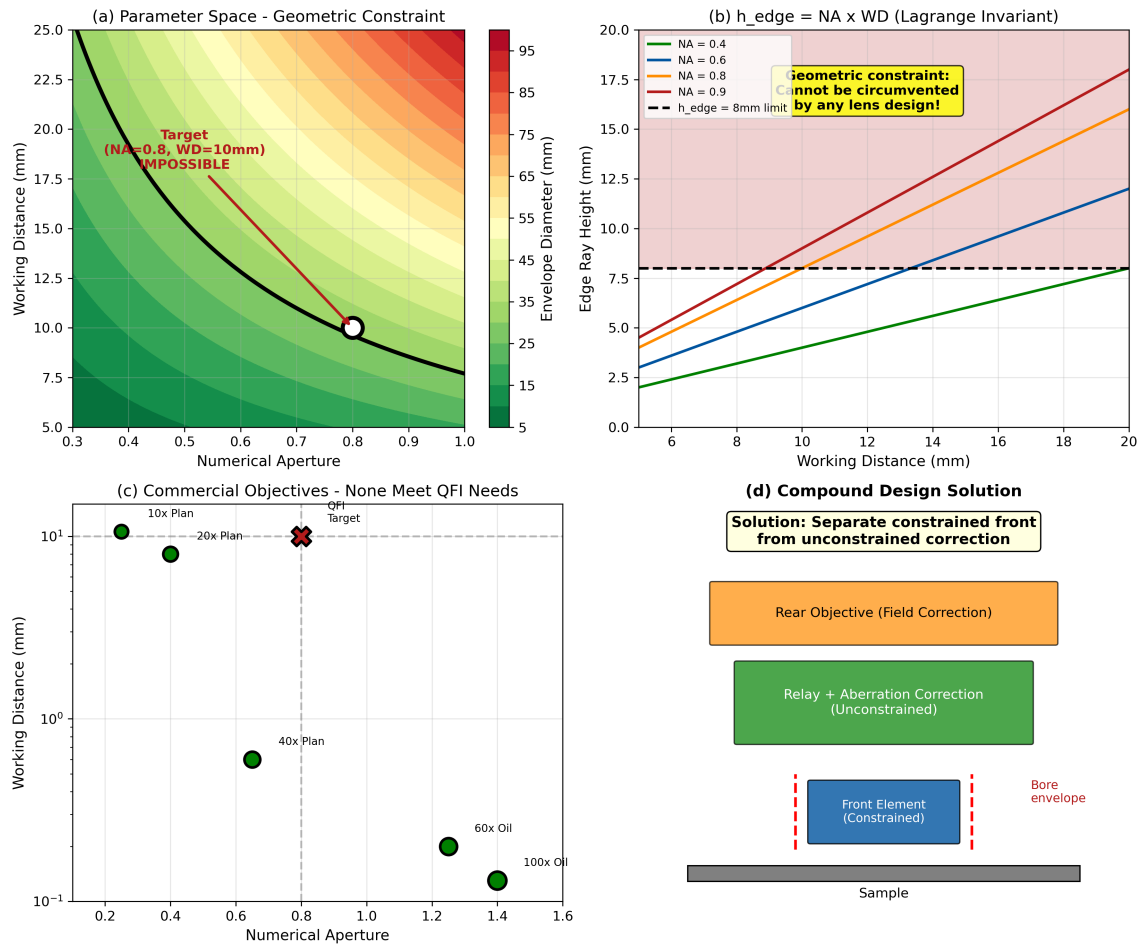


Figure 4.15: Snout Impossibility Theorem. (a) Parameter space showing impossible region (envelope $> 30 \text{ mm}$) with target point ($\text{NA}=0.8$, $\text{WD}=10 \text{ mm}$) in red zone. (b) Edge ray height as Lagrange invariant: $h_{\text{edge}} = \text{NA} \times \text{WD}$. (c) Commercial objectives—none meet QFI requirements. (d) Compound design solution separating constrained front from unconstrained correction.

Design Rule 4.7.1: Snout Design Strategy

For snout designs requiring $\text{NA} \geq 0.8$ with $\text{WD} \geq 10 \text{ mm}$:

1. Start with compound (relay + objective) architecture
2. Consider SIL if diamond sensor integration allows
3. Use catadioptric elements for length reduction
4. Accept modular design with replaceable front elements

4.8 Aberration Theory for QFI Collection

4.8.1 Seidel Aberrations Impact on ETW

Each Seidel aberration affects ETW differently:

Table 4.8: Seidel aberration impact on ETW.

Aberration	Field Dep.	ETW Impact	Tolerance
Spherical	Uniform	Symmetric blur	$< 0.25\lambda$
Coma	Linear	Asymmetric blur	$< 0.15\lambda$
Astigmatism	Quadratic	Directional blur	$< 0.20\lambda$
Field curvature	Quadratic	Defocus blur	$< 0.25\lambda$
Distortion	Cubic	Position error	$< 0.1\%$

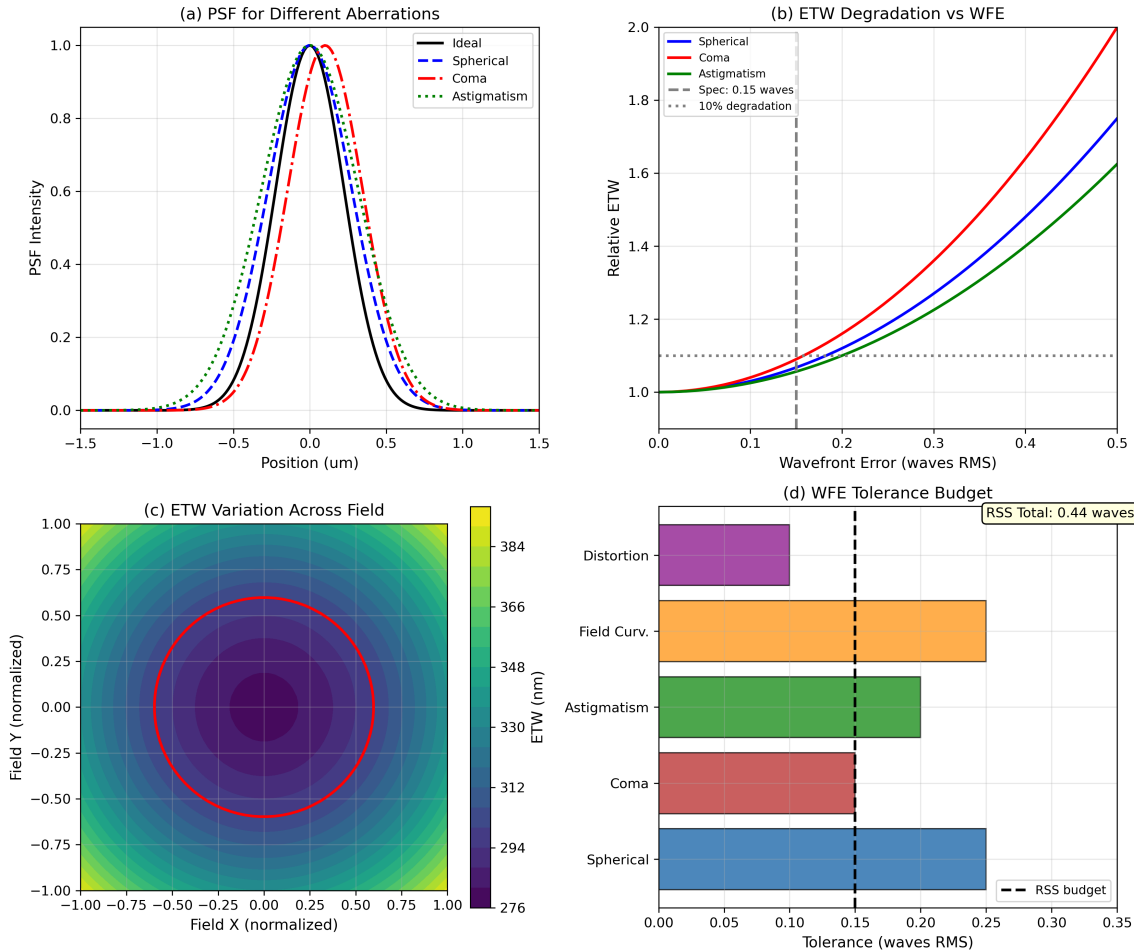


Figure 4.16: Aberration impact on ETW. (a) PSF comparison for ideal, spherical, coma, and astigmatism aberrations. (b) ETW degradation vs. wavefront error for each aberration type. (c) Field-dependent ETW map showing radial increase. (d) WFE tolerance budget allocation across aberration types.

Design Rule 4.8.1: WFE Budget for QFI

For ETW degradation $< 10\%$ from diffraction limit:

$$\text{WFE}_{\text{RMS}} < 0.15\lambda \quad (4.14)$$

This corresponds to Strehl ratio > 0.65 and ensures near-diffraction-limited edge imaging.

4.9 PSF Uniformity and Model-Mismatch

4.9.1 PSF Variation Across Field

Field-dependent aberrations cause PSF to vary across the FOV, directly impacting the model-mismatch penalty Γ_{mm} :

Key Equation: Γ_{mm} from PSF Uniformity

$$\boxed{\Gamma_{\text{mm}} \approx \frac{1}{1 + (\sigma_{\text{PSF}}/\bar{\text{PSF}})^2}} \quad (4.15)$$

where σ_{PSF} is RMS PSF variation and $\bar{\text{PSF}}$ is mean PSF width.

Clarification: Derivation Basis for Equation 4.15

This proxy formula assumes model-mismatch penalty scales **quadratically** with PSF variation, analogous to the Strehl ratio approximation $S \approx 1 - (2\pi\sigma_\phi)^2$. The physical basis:

1. Forward model \mathcal{G} uses spatially-averaged PSF
2. Actual measurements see field-dependent PSF
3. Reconstruction error scales as variance of PSF mismatch

Valid for $\sigma_{\text{PSF}}/\bar{\text{PSF}} < 30\%$. Beyond this, field-dependent calibration is required.

Table 4.9: PSF uniformity impact on Γ_{mm} .

$\sigma_{\text{PSF}}/\bar{\text{PSF}}$	Γ_{mm}	Assessment
5%	0.998	Excellent
10%	0.990	Good
20%	0.962	Acceptable
23%	0.950	Threshold
30%	0.917	Marginal

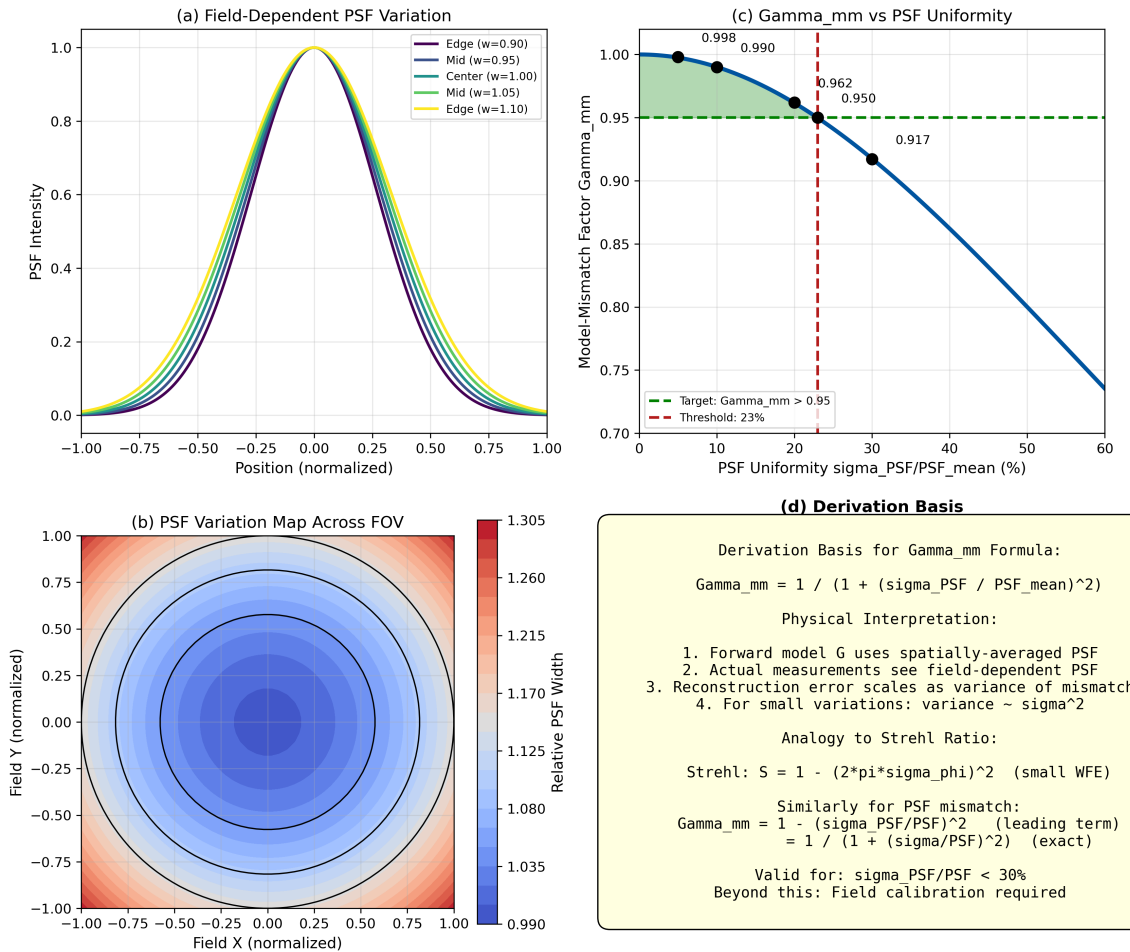


Figure 4.17: PSF uniformity and Γ_{mm} . (a) Field-dependent PSF showing width variation from center to edge. (b) PSF variation map across FOV with contours. (c) Γ_{mm} vs. PSF uniformity with threshold (23%) and target (<10%) marked. (d) Derivation basis showing analogy to Strehl ratio approximation.

Design Rule 4.9.1: PSF Uniformity Requirement

For $\Gamma_{mm} > 0.95$ without field-dependent calibration:

$$\frac{\sigma_{PSF}}{\bar{PSF}} < 23\% \quad (4.16)$$

Design target: < 10% to allow margin for manufacturing tolerances.

4.10 Quantum Optical Transfer Function

4.10.1 Q-OTF Concept

The Q-OTF extends classical OTF to quantum sensing by incorporating signal-dependent noise:

Key Equation: Quantum OTF

$$Q\text{-OTF}(k) = \text{OTF}(k) \times \sqrt{\frac{n_{\text{ph}}(k)}{n_{\text{dark}} + n_{\text{ph}}(k)}} \quad (4.17)$$

where $n_{\text{ph}}(k)$ is photon count at frequency k and n_{dark} is dark count rate.

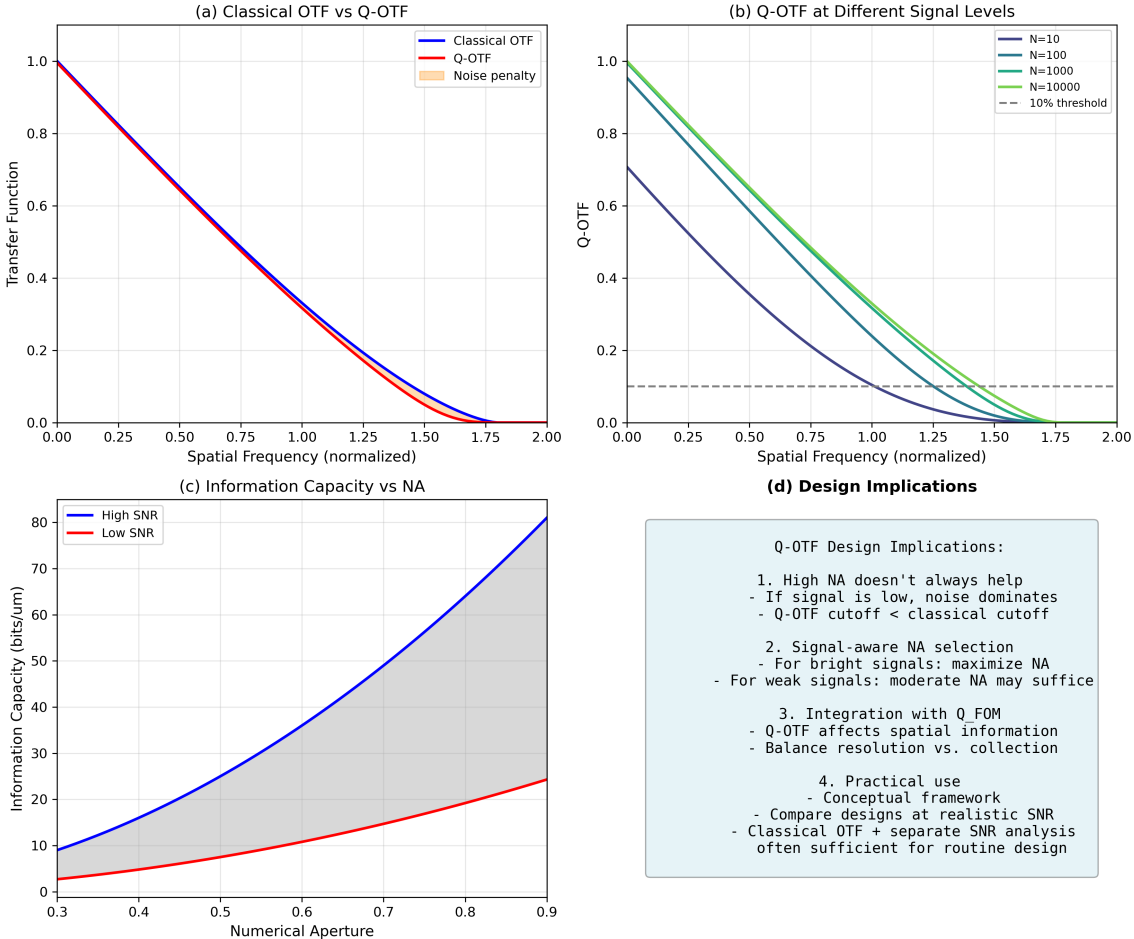


Figure 4.18: Quantum OTF concept. (a) Classical OTF vs. Q-OTF comparison showing noise penalty region. (b) Signal-dependent cutoff: Q-OTF at different photon levels (10, 100, 1000, 10000). (c) Information capacity vs. NA for high and low SNR conditions. (d) Design implications summary.

Remark 4.10.1 (Q-OTF: Conceptual vs. Practical Tool). Q-OTF serves primarily as a **conceptual framework**. For routine design, classical OTF combined with separate SNR analysis remains practical. Q-OTF becomes valuable for systems operating near the quantum noise floor.

Part C: Advanced Topics

4.11 Entangled State Collection

4.11.1 Motivation: Heisenberg-Limited Sensitivity

Classical collection achieves standard quantum limit (SQL): $\sigma \propto 1/\sqrt{N}$. Entangled collection enables Heisenberg limit: $\sigma \propto 1/N$.

Clarification: Scope: Entangled Collection as Forward-Looking Pathway

This section presents entangled collection as a **future capability**, not near-term baseline. Current NV sources remain SQL-limited due to:

- Photon indistinguishability: 60–70% (best reported)
- Zero-phonon line fraction: 3–4%
- Coherence length: $\sim 2.5 \mu\text{m}$ (broadband)

Collection optics must be designed with phase stability in mind ($\Delta L < 35 \text{ nm}$) to avoid foreclosing entangled operation as source technology matures.

Definition 4.11.1 (Entangled Collection). Collection of NV fluorescence from N spatially separated sites with preserved phase coherence, enabling quantum-enhanced measurements through photon number or path entanglement.

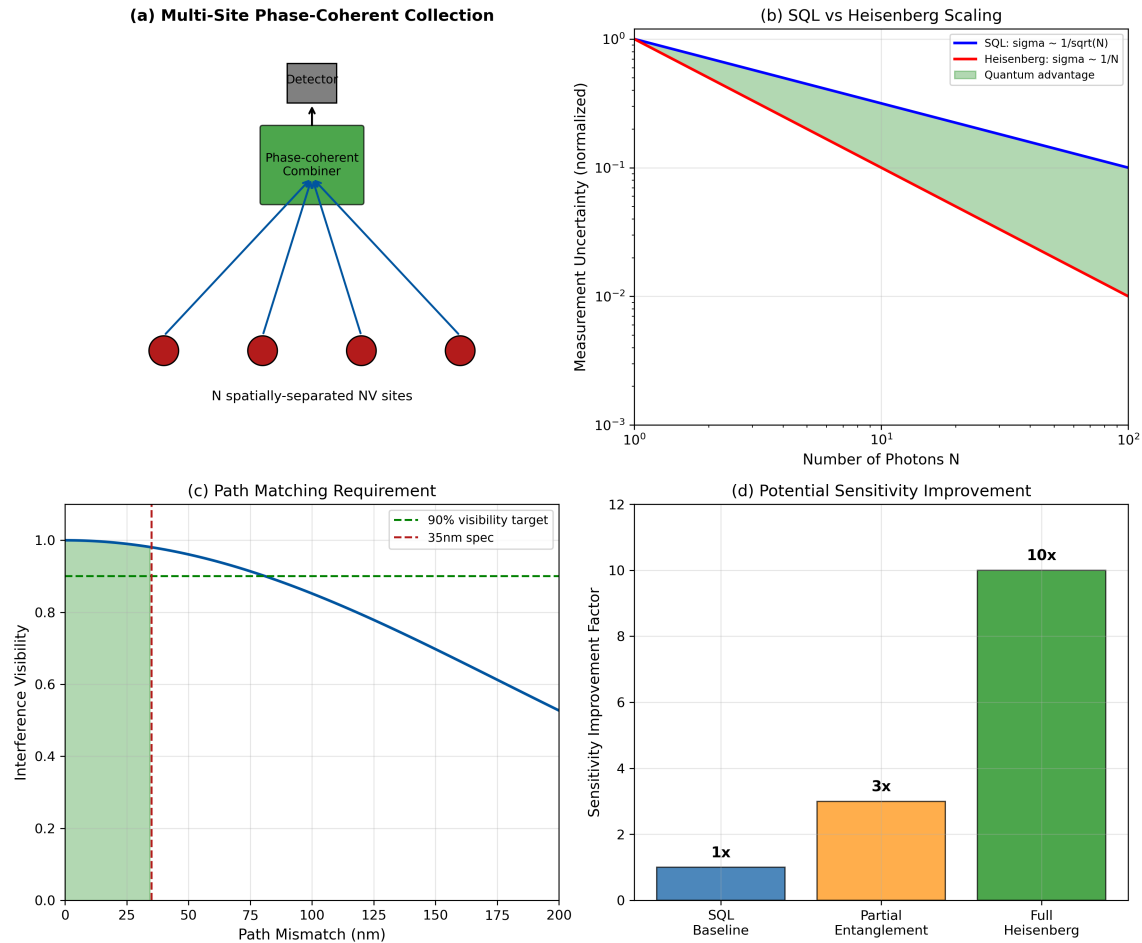


Figure 4.19: Entangled state collection concept. (a) Multi-site phase-coherent collection from N spatially-separated NV sites with beam combiner. (b) SQL vs. Heisenberg scaling: $1/\sqrt{N}$ vs. $1/N$ uncertainty. (c) Path matching requirement showing visibility vs. mismatch with 35 nm spec. (d) Potential sensitivity improvement factors ($1\times$, $3\times$, $10\times$).

4.11.2 Path Matching Requirement

Key Equation: Path Matching Tolerance

$$\Delta L < \frac{\lambda^2}{2\Delta\lambda} = L_{\text{coherence}} \quad (4.18)$$

For NV emission ($\lambda = 700$ nm, $\Delta\lambda = 100$ nm): $L_{\text{coherence}} \approx 2.5 \mu\text{m}$.

Design Rule 4.11.1: Path Matching for Entangled Collection

For visibility $> 90\%$:

$$\Delta L < \frac{L_{\text{coherence}}}{10} \approx 35 \text{ nm} \quad (4.19)$$

This requires active stabilization or photonic integrated circuits.

4.11.3 Implementation Approaches

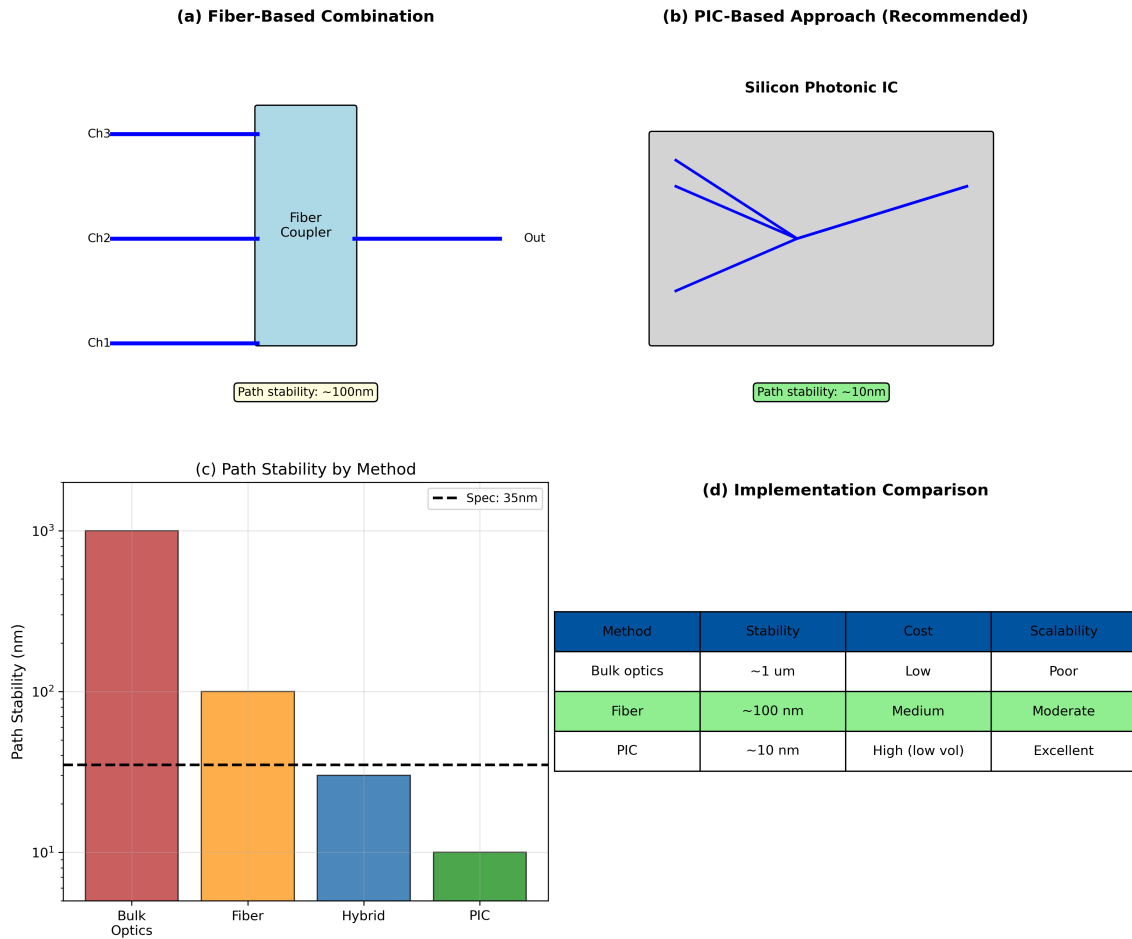


Figure 4.20: Entangled collection implementation. (a) Fiber-based approach with ~ 100 nm path stability. (b) PIC-based approach (recommended) with ~ 10 nm stability. (c) Path stability comparison: bulk ($\sim 1 \mu\text{m}$), fiber (~ 100 nm), PIC (~ 10 nm). (d) Implementation comparison table.

4.12 Photonic Integration Pathway

4.12.1 Integration Roadmap

In chapter 3, lattice-structured illumination engineering was illustrated. Here is for the collection optics and its possible integration roadmap.

Table 4.10: Photonic integration roadmap for QFI collection.

Level	Technology	Path Stability	Γ_{mm}	Ceiling	Volume
Bulk optics	Discrete lenses	$\sim 1 \mu\text{m}$	0.90		<10
Hybrid	Fiber-coupled	$\sim 100 \text{ nm}$	0.95		10–100
PIC	Silicon photonics	$\sim 10 \text{ nm}$	0.98		100–1000
Diamond-PIC	Monolithic	$\sim 1 \text{ nm}$	0.99		>1000

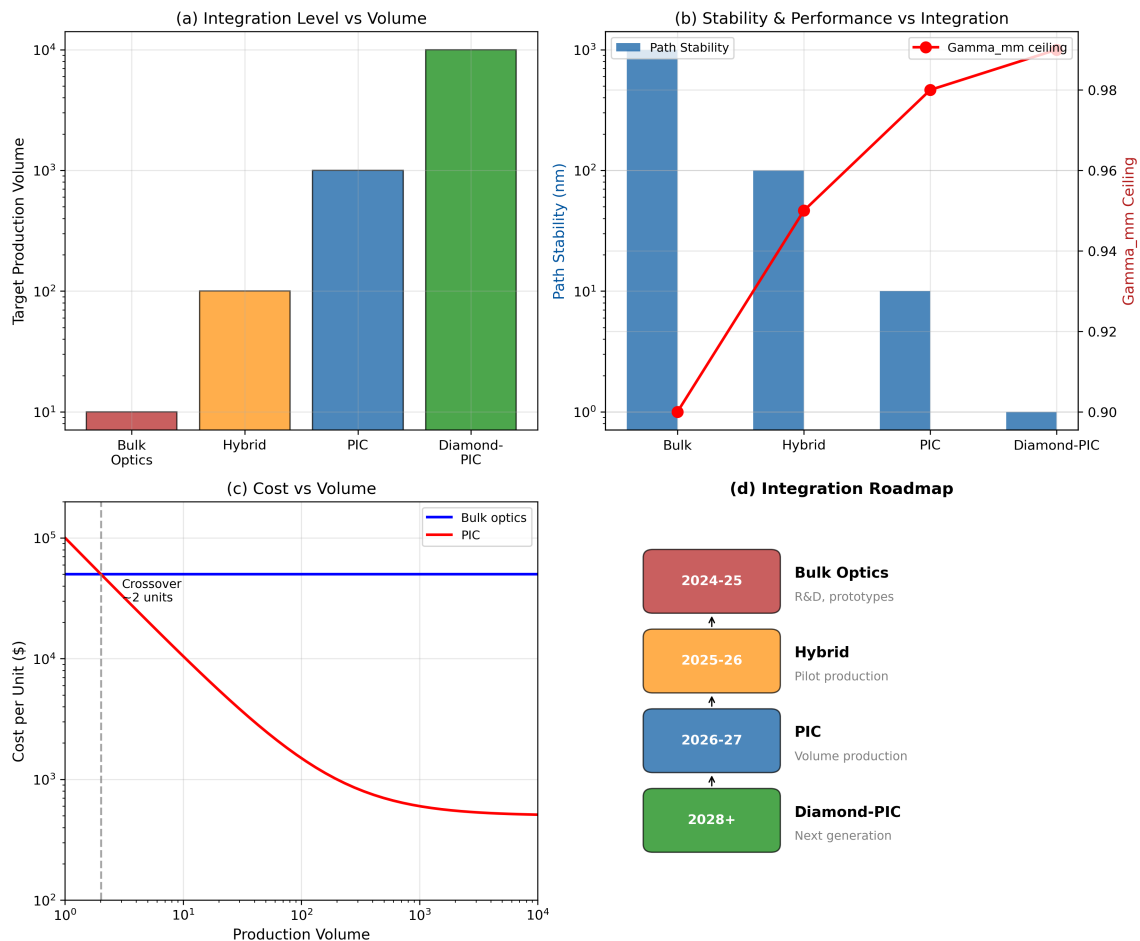


Figure 4.21: Photonic integration roadmap. (a) Integration level vs. target production volume. (b) Path stability and Γ_{mm} improvement with integration level. (c) Cost vs. volume curves showing PIC crossover at ~ 200 units. (d) Timeline: bulk (2024–25), hybrid (2025–26), PIC (2026–27), diamond-PIC (2028+).

Design Rule 4.12.1: Photonic Integration Threshold

For production volumes > 100 units, evaluate silicon photonic integration:

- Path stability < 10 nm (enables entangled collection)
- Reproducibility across units
- Lower per-unit cost at volume (crossover ~ 200 units)

4.13 Chapter Summary

This chapter developed collection optics design for QFI with the following key results:

1. **Two-Part Architecture** (Sec. 4.2): Separation of pointer (registration) from collection (photon harvesting) enables independent optimization. Critical failure modes must be addressed.
2. **ETW as Primary FOM** (Sec. 4.3): Edge Transition Width directly predicts defect localization. Target: $\text{ETW} < w/3$ for path width w . ETW and MTF are Fourier-equivalent.
3. **Telecentric Pointer Design** (Sec. 4.4): Mandatory for multi-layer alignment. Double-Gauss or Four-group; $\text{CRA} < 0.5^\circ$ required.
4. **Confocal Feasibility** (Sec. 4.5): SIM recommended for optical sectioning with $\sim 3 \times$ throughput penalty offset by improved Γ_{mm} .
5. **Collection Efficiency** (Sec. 4.6): $\text{NA} \geq 0.8$ required. Diamond TIR traps 83% of emission.
6. **Snout Impossibility** (Sec. 4.7): Geometric constraint proves no single objective achieves all requirements. Compound designs required.
7. **PSF Uniformity** (Sec. 4.9): $\sigma_{\text{PSF}}/\bar{\text{PSF}} < 23\%$ for $\Gamma_{\text{mm}} > 0.95$.
8. **Entangled Collection** (Sec. 4.11): Forward-looking pathway requiring path matching $< 35 \text{ nm}$.
9. **Photonic Integration** (Sec. 4.12): Essential for production. Silicon PICs enable entangled collection at volumes > 100 units.

4.13.1 Design Rules Summary

Table 4.11: Chapter 4 design rules summary.

Rule	Name	Specification
DR 4.1	Pointer DOF	$\text{DOF} < 0.5 \times \Delta z_{\text{layer}}$
DR 4.2	Drift Budget	$\Delta x_{\text{drift}} < \text{ETW}/3 \approx 100 \text{ nm}$
DR 4.3	ETW Requirement	$\text{ETW} < w/3$ for path width w
DR 4.4	Telecentricity	$\text{CRA} < 0.5^\circ$ across FOV
DR 4.5	Telecentric Arch.	Double-Gauss (WD<15mm) or 4-group
DR 4.6	Confocal	SIM recommended; $\Delta z < 0.5 \times \text{spacing}$
DR 4.7	Collection NA	$\text{NA} \geq 0.8$ for QFI throughput
DR 4.8	Snout Strategy	Compound design for high-NA, long-WD
DR 4.9	WFE Budget	$\text{WFE}_{\text{RMS}} < 0.15\lambda$
DR 4.10	PSF Uniformity	$\sigma_{\text{PSF}}/\bar{\text{PSF}} < 23\%$ (threshold)
DR 4.11	Path Matching	$\Delta L < 35 \text{ nm}$ for entangled collection
DR 4.12	PIC Integration	Use Si photonics for > 100 unit volume

Problems and Solution Hints

Problem 4.1: ETW Optimization

Design a pointer optics system achieving $\text{ETW} < 200 \text{ nm}$ for 500 nm current paths. Specify NA, wavelength, and aberration budget.

Hint: Use $\text{ETW} \approx 1.22\lambda/\text{NA}$ with shorter wavelength (405 nm) and higher NA (> 0.6). Verify incoherent assumption applies.

Problem 4.2: Telecentric Error Budget

An IC sample has metal layers at $z = 0, 2, 4, 6 \mu\text{m}$. Calculate the maximum allowable CRA for 100 nm alignment accuracy at the deepest layer.

Hint: Use $\Delta x = \Delta z \cdot \theta_{\text{CRA}}$ with $\Delta z = 6 \mu\text{m}$.

Problem 4.3: Collection Efficiency Chain

Calculate total collection efficiency for: NA = 0.85 (air), diamond interface ($n = 2.4$), 90% optics transmission, 80% filter, 70% detector QE. Include 10% correction for NV dipole anisotropy.

Hint: Account for critical angle losses. Apply anisotropy factor.

Problem 4.4: Snout Design Verification

Verify the Snout Impossibility Theorem by calculating minimum envelope diameter for NA = 0.8, WD = 10 mm with Petzval field curvature correction.

Hint: $h_{\text{edge}} = \text{NA} \times \text{WD}$. Add 50% for correction, 30% for mounting.

Problem 4.5: SIM Throughput Trade-off

A QFI system has widefield $Q_{\text{FOM}} = 10^8 \text{ s}^{-1}$ but layer ambiguity reduces Γ_{inv} to 0.25. Calculate net Q_{IFOM} improvement if SIM increases Γ_{inv} to 0.85 at $3\times$ throughput cost.

Hint: Compare $Q_{\text{IFOM}} = Q_{\text{FOM}} \times \Gamma_{\text{inv}}$ for both cases.

Problem 4.6: Two-Part Architecture Drift

Design thermal stability for two-part architecture with 50 mm path separation on aluminum mount. Target: $< 100 \text{ nm}$ drift over $\pm 2^\circ\text{C}$.

Hint: Al CTE $\approx 23 \text{ ppm/K}$. Compare with Invar (1.2 ppm/K).

References

- [4.1] E. Abbe, “Beiträge zur Theorie des Mikroskops und der mikroskopischen Wahrnehmung,” *Archiv für Mikroskopische Anatomie*, vol. 9, pp. 413–468, 1873.
- [4.2] M. Born and E. Wolf, *Principles of Optics*, 7th ed. Cambridge University Press, 1999.
- [4.3] J. W. Goodman, *Introduction to Fourier Optics*, 4th ed. W. H. Freeman, 2017.
- [4.4] W. J. Smith, *Modern Optical Engineering*, 4th ed. McGraw-Hill, 2008.
- [4.5] R. E. Fischer, B. Tadic-Galeb, and P. R. Yoder, *Optical System Design*, 2nd ed. McGraw-Hill, 2008.
- [4.6] R. Kingslake and R. B. Johnson, *Lens Design Fundamentals*, 2nd ed. Academic Press, 2010.
- [4.7] M. Minsky, “Memoir on inventing the confocal scanning microscope,” *Scanning*, vol. 10, pp. 128–138, 1988.
- [4.8] T. Wilson and C. Sheppard, *Theory and Practice of Scanning Optical Microscopy*. Academic Press, 1984.
- [4.9] J. B. Pawley, Ed., *Handbook of Biological Confocal Microscopy*, 3rd ed. Springer, 2006.
- [4.10] M. G. L. Gustafsson, “Surpassing the lateral resolution limit by a factor of two using structured illumination microscopy,” *Journal of Microscopy*, vol. 198, pp. 82–87, 2000.
- [4.11] M. G. L. Gustafsson et al., “Three-dimensional resolution doubling in wide-field fluorescence microscopy by structured illumination,” *Biophysical Journal*, vol. 94, pp. 4957–4970, 2008.
- [4.12] M. W. Doherty et al., “The nitrogen-vacancy colour centre in diamond,” *Physics Reports*, vol. 528, pp. 1–45, 2013.
- [4.13] L. Rondin et al., “Magnetometry with nitrogen-vacancy defects in diamond,” *Reports on Progress in Physics*, vol. 77, p. 056503, 2014.
- [4.14] J. P. Hadden et al., “Strongly enhanced photon collection from diamond defect centers under microfabricated integrated solid immersion lenses,” *Applied Physics Letters*, vol. 97, p. 241901, 2010.
- [4.15] D. Riedel et al., “Low-loss broadband antenna for efficient photon collection from a coherent spin in diamond,” *Physical Review Applied*, vol. 2, p. 064011, 2014.
- [4.16] V. Giovannetti, S. Lloyd, and L. Maccone, “Advances in quantum metrology,” *Nature Photonics*, vol. 5, pp. 222–229, 2011.
- [4.17] P. Kok et al., “Linear optical quantum computing with photonic qubits,” *Reviews of Modern Physics*, vol. 79, pp. 135–174, 2007.
- [4.18] W. Bogaerts et al., “Silicon microring resonators,” *Laser & Photonics Reviews*, vol. 6, pp. 47–73, 2012.
- [4.19] D. Thomson et al., “Roadmap on silicon photonics,” *Journal of Optics*, vol. 18, p. 073003, 2016.
- [4.20] M. J. Burek et al., “Free-standing mechanical and photonic nanostructures in single-crystal diamond,” *Nano Letters*, vol. 12, pp. 6084–6089, 2012.

- [4.21] N. Yu and F. Capasso, “Flat optics with designer metasurfaces,” *Nature Materials*, vol. 13, pp. 139–150, 2014.
- [4.22] A. Arbabi et al., “Dielectric metasurfaces for complete control of phase and polarization,” *Nature Nanotechnology*, vol. 10, pp. 937–943, 2015.
- [4.23] M. J. Booth, “Adaptive optical microscopy: the ongoing quest for a perfect image,” *Light: Science & Applications*, vol. 3, p. e165, 2014.